Naval Ocean Systems Center
San Diego, CA 92152-5000

Technical Document 1706
November 1989

Analytic Parabolic Equation Solutions

Science and Technology Corporation

NAVAL OCEAN SYSTEMS CENTER

San Diego, California 92152-5000

J. D. FONTANA, CAPT, USN
Commander

R. M. HILLYER
Technical Director

ADMINISTRATIVE INFORMATION

Contract N66001-88-D-0115 was carried out by the Science and Technology Corporation, 101 Research Drive, Hampton, VA 23666-1340, under the technical coordination of N. M. Vorce, Ocean and Atmospheric Sciences Division, Code 54, Naval Ocean Systems Center, San Diego, CA 92152-5000.

Released under authority of
J. H. Richter, Head
Ocean and Atmospheric Sciences Division

FS

REPORT DOCUMENTATION PAGE

Form Approved
OMB No. 0704-0188

1. AGENCY USE ONLY (Leave blank)	2. REPORT DATE	3. REPORT TYPE AND DATES COVERED
	November 1989	Final

4. TITLE AND SUBTITLE
ANALYTIC PARABOLIC EQUATION SOLUTIONS

5. FUNDING NUMBERS
C: N66001-88-D-0115

6. AUTHOR(S)

7. PERFORMING ORGANIZATION NAME(S) AND ADDRESS(ES)
Science and Technology Corporation
101 Research Drive
Hampton, VA 23666-1340

8. PERFORMING ORGANIZATION REPORT NUMBER
3021

9. SPONSORING/MONITORING AGENCY NAME(S) AND ADDRESS(ES)
Naval Ocean Systems Center
San Diego, CA 92152-5000

10. SPONSORING/MONITORING AGENCY REPORT NUMBER
NOSC TD 1706

11. SUPPLEMENTARY NOTES

12a. DISTRIBUTION/AVAILABILITY STATEMENT
Approved for public release; distribution is unlimited.

12b. DISTRIBUTION CODE

13. ABSTRACT (Maximum 200 words)

This document presents a Gaussian beam (GB) method for underwater acoustic propagation, with emphasis on critical reflection and head wave modeling due to a high velocity bottom.

14. SUBJECT TERMS
Gaussian beam (GB)
fast fluid bottom

15. NUMBER OF PAGES
59

16. PRICE CODE

17. SECURITY CLASSIFICATION OF REPORT	18. SECURITY CLASSIFICATION OF THIS PAGE	19. SECURITY CLASSIFICATION OF ABSTRACT	20. LIMITATION OF ABSTRACT
UNCLASSIFIED	UNCLASSIFIED	UNCLASSIFIED	

Section I

Summary of Accomplishments

I. Summary of Accomplishments

Under this Task, the following problem areas have been addressed:

1. Gaussian beam (GB) method for underwater acoustic propagation, with emphasis on critical reflection and head wave modeling due to a high velocity bottom.

   The objective here is to improve the narrow-waisted paraxial Gaussian beam (PA-GB) algorithm, which is computationally efficient but does not account for the total reflection-head wave phenomena. A test problem involving a line source in a homogeneous ocean above a homogeneous, semi-infinite, fast fluid bottom has been analyzed in detail. Various options for augmenting the deficient PA-GB stack have been proposed, examined and compared with a rigorous numerical reference solution.

   Details of the analysis and results obtained so far are given in Section II. This investigation will continue under a separate Task.

2. Hybrid ray-mode-PE method for high-frequency propagation in a tropospheric surface duct.

   The objective in this investigation is to improve the ray prediction code now in use at NOSC by self-consistent hybrid ray-mode-PE parametrization in those observational regions where ray theory fails. The canonical model is a line-source-excited duct with laterally homogeneous bilinear height profile. An exact numerical reference solution can be constructed by modal summation for comparison with the results obtained from the hybrid algorithm.

   The theory has been developed and is reported in Section III. Numerical implementation has been initiated and will be continued under a separate Task.

3. In addition to performing the technical tasks described under 1 and 2, substantial effort has been exerted on the preparation of manuscripts suitable for publication. The material in Secs. II and III has been written up in such a manner as to suit this objective. Each section is complete in itself and any references within the text refer to that section only.

II. Personnel

The following personnel have contributed under this Task:

Leopold B. Felsen

T. Ishihara

X.J. Gao

Section II

Spectral Options to Improve the Paraxial Narrow Gaussian Beam Algorithm for Critical Reflection and Head Waves

Spectral Options To Improve the Paraxial Narrow Gaussian Beam Algorithm for Critical Reflection and Head Waves

X.J. Gao and L.B. Felsen

I. Introduction

Wave propagation over long distances in complex surroundings that vary slowly over the scale of the local wavelength is of importance in many disciplines dealing with the terrestrial environment. Direct numerical methods are unsuitable because the problem is computationally large. Therefore, analytical models based on various types of propagators have been explored to render the problem tractable -- an exercise that requires a trade-off between analytical approximations and numerical complexity. Ray methods are favored in propagation algorithms because they are easily implemented numerically, but they suffer deficiencies in ray field transition regions associated with focusing effects (caustics and foci), shadow boundaries, diffraction, critical reflection, etc. These defects can be formally removed on replacing the ray fields with paraxial (PA) Gaussian beam fields (GB), because such beams do not fail in transitional domains, and tracking them numerically is only slightly more cumbersome than ray tracking. Moreover, by an extension of real ray theory, the PA Gaussian beam can be modeled as a bundle of complex rays emanating from a complex source point (CSP), thereby permitting its tracking through a simple extension of the procedures for real rays. These aspects have been well documented in the literature [1]. Since the final field is constructed by beam shooting, one avoids the need for eigenray search which would connect the CSP and the observer along a direct complex ray path. Instead, the field at the observer is synthesized by paraxial expansion about each on-axis beam field (each beam axis follows a real ray), thereby simplifying the algorithm substantially.

The major task in employing any scenario for propagation modeling is to assess its accuracy. This has to be done by comparing data from the proposed algorithm with data from an independently generated "reliable" solution, preferably a "benchmark" with known accuracy. The simplest benchmarks are draped around idealized canonical configurations that incorporate relevant wave phenomena within a formally exact, and numerically computable, framework. If discrepancies arise, careful study of these canonical solutions may reveal the reasons behind the shortcomings of the approximate model, and ways to repair the deficiencies.

In the PA-GB stacking scheme, one of the critical beam parameters is the beam waist. Wide-waisted beams (in terms of wavelength) have good PA behavior but are difficult to propagate through a complex environment, whereas the opposite is true for narrow-waisted beams. Even if defects can be tuned out initially by numerical experiment, such tuning generally will not remain intact as the beams progress through various refraction, reflection, diffraction, etc., encounters. For many applications, especially in seismology and bottom interacting ocean acoustics, critical

reflection and generation of head waves play an important role. Narrow PA-GB methods are known to fail here [2]. A detailed canonical prototype study has been performed previously to identify the cause of the failure: narrow PA-GB are spectrally deficient in their ability to cover both the specularly reflected and head wave contributions, whereas wide PA-GB are not [3]. However, wide PA-GB, as noted above, are numerically inefficient and cannot be well adapted to non-canonical propagation events.

In the present study, we have returned to the PA narrow beam critical angle problem for a line-source-excited critically reflecting interface separating two homogeneous half spaces (either for horizontally polarized shear (SH) waves in elastic, or for compressional (P) waves in fluid, environments), searching for ways in which to flesh out the deficient spectra without sacrificing the PA assumption. As may be anticipated, this endeavor turns out to be accompanied only with partial success. Initially, the investigation has been concerned with assessing the following options: 1. inclusion of the lateral (head) wave in the total reflection domain, outside the critical reflection transition region, where lateral wave asymptotics is invalid [4];2. inclusion of lateral shifts in the reflected beam fields, thereby yielding in the critical reflection domain two reflected contributions (one launched near the critical, and one near the specular, angle). 3. inclusion of the lateral wave and one (the near-specular) laterally shifted reflected ray. By systematic PA asymptotics as well as justifiable phenomenological considerations, each of these options accounts for the critical reflection and lateral wave effects individually. For the laterally shifted beams, the interface plane wave reflection coefficient is incorporated into the phase, and the resulting phase is made stationary to determine the beam axis trajectory. Numerical integration of the exact spectral integral has been taken as the the reference solution, with which these options are compared.

In these studies, the PA was retained in its conventional form wherein the phase at an off-axis observation point with respect to a particular beam in the stack is evaluated by perturbation (up to second order in the off-axis distance) about the on-axis field. The results still showed deficiencies, which were felt to be attributable, at least in part, to the conventional PA scheme, which is strained beyond its limits for narrow-waisted beams. To improve the approximation without sacrificing beam shooting, the off-axis results were recalculated by retaining the exact complex distance from the CSP to the observer. This modification, which can easily be incorporated into the algorithm, has been found to reduce the discrepancies with the reference solution, and it is therefore recommended. .

In what follows, the spectral integral reference solution is stated in Sec. II. Section III summarizes the PA-GB algorithm, both in its conventional (paraxial CSP) and improved (full CSP) versions. The augmentations of PA-GB described by options 1.-3. above are treated in Sec. IV, and the corresponding numerical comparisons for typical samples extracted from an extensive set of data are discussed in Sec. V. Concluding remarks are found in Sec. VI.

II. Spectral Integral Reference Solution

We consider acoustic wave propagation in the presence of a plane interface (z=0) that separates an upper half space (z > 0; medium 1) from a lower half space (z < 0 ; medium 2) (Fig. 1). Time-harmonic excitation (with suppressed dependence exp(-$i\omega t$) is from a y-directed line source located at (x_s, z_s). By plane wave spectral decomposition, at an observation point (x,z) in medium 1, the total field due to the interface is given by [5],

$$I = \frac{-1}{4\pi i} \int_{-\infty}^{\infty} \frac{\Gamma(\xi)}{\kappa_1(\xi)} e^{i\psi(\xi)} d\xi \qquad (1)$$

where the integration path is shown in Fig. 2(a), ξ is the spectral parameter (wavenumber along x) in the plane wave continuum,

$$\psi(\xi) = \xi(x-x_s) + \kappa_1(z+z_s),\ \kappa_i(\xi) = \sqrt{k_i^2 - \xi^2},\quad \mathrm{Im}\,(\kappa_i)>0,\ i = 1,2 \qquad (1a)$$

and

$$\Gamma(\xi) = \frac{A_1\kappa_1(\xi) - A_2\kappa_2(\xi)}{A_1\kappa_1(\xi) + A_2\kappa_2(\xi)}\ ,\quad \begin{cases} A_i = \rho_i v_i^2,\ i = 1,2 \text{ for SH waves (elastic)} & (1b) \\ A_1 = \rho_2, A_2 = \rho_1 \text{ for P waves (fluid)} & (1c) \end{cases}$$

is the interface reflection coefficient. The wave propagation speeds in medium 1 and 2 are v_1 and v_2, respectively, the corresponding wavenumbers are $k_{1,2} = \omega/v_{1,2}$, and the densities are $\rho_{1,2}$. An angular spectrum reprsentation in terms of the angle θ (Fig. 2(b)) is obtained via the mapping

$$\xi = k_1 \sin\theta \qquad (2)$$

The integration contours in the complex ξ and θ planes, consonant with the radiation condition, are shown in Fig. 2.

III. The Gaussian Beam Method

The conventional GB method [1], whose formulations have been critically examined in [5] and [6], is briefly summarized here. By that method, the incident field from the line source is approximated by a continuum of PA-GB whose amplitudes are adjusted so as to reproduce the asymptotic far field from the exact angular spectrum (see (1), with (2), and Γ replaced by 1). The angular spectrum PA-GB integral is then discretized for numerical evaluation, with $\Delta\alpha$ denoting the angular separation between adjacent beams, which are assigned a beam waist $w_0 = (2b/k_1)^{1/2}$, with b denoting a parameter equivalent to the Fresnel length. b and $\Delta\alpha$ are at the disposal of the user, and this is at the root of the arbitrariness that besets this method [6]. Considering

propagation to the right as in Fig. 3(a), the angular spectrum interval may be truncated at $\alpha^{(1)}$ and $\alpha^{(2)}$, assuming (subject to numerical test) that beams outside that interval make a negligible contribution. This leads to the following PA-GB expansion of the integral (1):

$$I \sim \sum_{\alpha^{(1)}}^{\alpha^{(2)}} \Phi_n G_n \Delta\alpha \ , \ -\frac{\pi}{2} \le \alpha_1 < \alpha_2 \le \frac{\pi}{2}, \ \ \Delta\alpha << 1 \tag{3}$$

Each incident and reflected-GB can be modeled by a source at a complex location (CSP), with the complex displacement for a given beam waist specified by the parameter b. Since the asymptotic reflected field derived from the spectral integral in (1) is equivalent to the field emanating from an image source located as in Fig. 3(b) in the infinitely extended medium 1, with the strength of the image source given by the spectral reflection coefficient Γ, one may write the full CSP asymptotic approximation for each reflected beam as follows [5]:

$$\Phi_n \equiv \Phi(\alpha_n) = \Phi(0) = \frac{\sqrt{k_1(b-iS)}}{2\pi} \exp(ik_1 S - k_1 b) \tag{3a}$$

$$G_n \equiv \frac{-1}{4\pi i} \Gamma(k_1 \sin\tilde{\theta}_n) \left[\frac{2\pi}{k_1 \tilde{R}_n}\right]^{\frac{1}{2}} \exp\left[ik_1 \tilde{R}_n - \frac{i\pi}{4}\right] \tag{3b}$$

where $\tilde{R}_n$ is the complex radial distance from the n-th beam waist center to the observer at (x,z),

$$\tilde{R}_n = \sqrt{(x-\tilde{x}_{sn})^2 + (z+\tilde{z}_{sn})^2}, \ \ \mathrm{Re}(\tilde{R}_n) > 0 \tag{3c}$$

and $\tilde{\theta}_n$ denotes the complex observation angle given by

$$\sin\tilde{\theta}_n = \frac{x-\tilde{x}_{sn}}{\tilde{R}_n} \tag{3d}$$

The beams are launched from the initial surface with radius S in the "far zone" of the line source located at (x_s, z_s). The n-th beam waist center on s is located at (x_{sn}, z_{sn}), where (see Fig. 3(a))

$$x_{sn} = x_s + S\sin\alpha_n, \ z_{sn} = z_s + S\cos\alpha_n \tag{3e}$$

with α_n denoting angular location. In terms of these quantities, the corresponding CSP $(\tilde{x}_{sn}, \tilde{z}_{sn})$ for the n-th beam is given by

$$\tilde{x}_{sn} = x_{sn} + ib\sin\alpha_n, \ \ \tilde{z}_{sn} = z_{sn} + ib\cos\alpha_n \tag{3f}$$

The complex coordinates are schematized in Fig. 3.

The conventional PA is recovered from the full CSP result in (3b) by the following approximations:

1. expanding $\tilde{R}_n$ in the phase to second order in the off-axis distance d_n:

$$\tilde{R}_n \approx \tilde{R}_{an} + \frac{1}{2}\frac{d_n^2}{r_{an} - ib} \tag{4a}$$

2. expanding $\tilde{R}_n$ in the amplitude factor to first order:

$$\tilde{R}_n \approx \tilde{R}_{an} \tag{4b}$$

3. replacing the complex angle $\tilde{\theta}_n$ by the real beam angle α_n in the reflection coefficient Γ:

$$\Gamma(k_1 \sin\tilde{\theta}_n) \approx \Gamma(k_1 \sin\alpha_n) \tag{4c}$$

With reference to Fig. 3(a), one identifies the various geometrical quantities: d_n is the perpendicular displacement from the point (x_{an}, z_{an}) on the beam axis along α_n to the observer at (x,z), while r is the radial distance from the image source to (x,z) and θ is its angular displacement from the z-axis. Explicit expressions for, and relations between, these quantities are:

$$r = \sqrt{r_{a0}^2 + d_0^2}\ , \theta = \alpha_0 + \tan^{-1}\left(\frac{d_0}{r_{a0}}\right) \tag{4d}$$

where $d_0 > 0$ if $x > x_{a0}$, $d_0 < 0$ if $x < x_{a0}$

$$d_n = r \sin(\theta - \alpha_n) \tag{4e}$$

$$r_{an} = r\cos(\theta - \alpha_n) - S \tag{4f}$$

$$x_{an} = x_s + r\sin\alpha_n\ ,\ z_{an} = z_s + \tag{4g}$$

Thus, the complex radial distance to (x_{an}, z_{an}) is

$$\tilde{R}_{an} = \sqrt{(x_{an} - \tilde{x}_{sn})^2 + (z_{an} + \tilde{z}_{sn})^2},\ \mathrm{Re}(\tilde{R}_{an}) > 0 \tag{4h}$$

Implementation of the algorithm in (3) via the conventional PA-GB model in 4(a)-4(h), leads to the difficulties discussed in [5]. For narrow-waisted beams, substantial discrepancies exist between the PA-GB and reference solutions, with the

former missing essentially the (reflected wave) - (head wave) interference. This can be attributed to the inability of the narrow PA-GB spectrum to account for both wave phenomena. It is therefore suggested to augment the algorithm in (3) by including each of these phenomena individually. The options to be pursued have been noted in Section I. Subsequently, we shall show that the full CSP-GB reduces the discrepancies.

IV. Augmented Conventional PA-GB Method

A. PA-GB plus head wave

In this option, we include the head wave contribution excited by the n-th conventional PA-GB in (3), with (4). The domain of existence of the n-th head wave can be ascertained by returning to the exact spectral integral for the line source in (1), changing the line source input into the n-th GB input through replacement of the real source coordinate (x_s,z_s) by the n-th beam complex source (CSP) coordinate $(\tilde{x}_{sn},\tilde{z}_{sn})$, and performing an asymptotic evaluation of the resulting exact integral for the total field excited by the n-th incident GB. This requires deformation of the original integration path into the steepest descent path (SDP) through the complex saddle point ξ_n (Fig. 2). If the branch point at $\xi_b = k_2$ is intercepted during this deformation, (this occurs, roughly speaking, for observation angles $\theta>\theta_c$, where $\theta_c = \sin^{-1}(v_1/v_2)$ is the angle of critical reflection), a branch cut contribution I_{bn} must be added to the SDP contribution; asymptotically, the former generates the reflected GB I_{sn} whereas the latter generates the head wave excited by that GB. Asymptotics are valid when the branch point and saddle point are sufficiently well separated. A measure of the separation is provided by the numerical distance ND, and it has been found that $ND\geq 2$ is adequate.

A detailed discussion is given in [5]. Correcting the omission of the density and velocity ratio in the SH wave formula of that paper (the correct formula is given in (1b)), it is found that the contribution excited by the n-th incident beam is given by:

$$I_n = I_{sn} + I_{bn}\, U(\xi_r - k_2) \tag{5}$$

$$U(x) = \begin{cases} 0 & x<0 \\ 1/2 & x=0 \\ 1 & x>0 \end{cases} \tag{5a}$$

where ξ_r denotes the intersection of the SDP with the real axis in the complex ξ-plane, and $I_{sn} \equiv G_n$ is given in (3b). The branch point contribution is given by

$$I_{bn} \sim -\frac{1}{\sqrt{2\pi}}\,\frac{A_2}{A_1}\,\frac{\sqrt{\tan\theta_c}}{(k_1\tilde{R}_n \sin\tilde{\Delta}_n)^{3/2}}\, e^{ik_1\tilde{R}_n\cos\tilde{\Delta}_n - i\frac{\pi}{4}} \tag{5b}$$

The following definitions have been used here,

$$\sin\tilde{\Delta}_n = \frac{x-\tilde{x}_{sn}}{\tilde{R}_n}\cos\theta_c - \frac{z+\tilde{z}_{sn}}{\tilde{R}_n}\sin\theta_c \tag{5c}$$

$$\cos\tilde{\Delta}_n = \frac{x-\tilde{x}_{sn}}{\tilde{R}_n}\sin\theta_c + \frac{z+\tilde{z}_{sn}}{\tilde{R}_n}\cos\theta_c \tag{5d}$$

$$\mathrm{Re}\,[k_1\tilde{R}_n\sin\tilde{\Delta}_n]^{3/2} > 0 \tag{5e}$$

The numerical distance is given by [7],

$$ND = |\tilde{\zeta}| \tag{5f}$$

where

$$\tilde{\zeta} = i(-2ik_1\tilde{\gamma})^{\frac{1}{2}}\,\frac{\tilde{\beta}}{2\tilde{\gamma}} \tag{5g}$$

$$\tilde{\beta} = \left[\sin\theta_c\left(\frac{z+\tilde{z}_{sn}}{\tilde{R}_n}\right) - \cos\theta_c\left(\frac{x-\tilde{x}_{sn}}{\tilde{R}_n}\right)\right] \Big/ \sin 2\theta_c \tag{5h}$$

$$\tilde{\gamma} = -\frac{1}{8}\left(\frac{z+\tilde{z}_{sn}}{\tilde{R}_n\cos^3\theta_c} + \frac{x-\tilde{x}_{sn}}{\tilde{R}_n\sin^3\theta_c}\right) \tag{5i}$$

$$\theta_c = \sin^{-1}\left(\frac{v_1}{v_2}\right) \tag{5j}$$

and $\tilde{R}_n$ is given by (3c).

B. Laterally shifted PA-GB

This option is based on an alternative procedure for the asymptotic evaluation of the spectral integral (1). Instead of treating the reflection coefficient Γ as a spectral

amplitude as in Sec. IV A, it is now incorporated into the phase via the identity $\Gamma = \exp(\not\angle n\,\Gamma)$, [8]. This alters the stationary phase (saddle point) condition and yields modified reflected ray trajectories that contain an additional path segment.

For a ray incident beyond the critical angle ($\theta > \theta_c$), $\not\angle n\,\Gamma$ is imaginary and the additional segment can be interpreted as a real lateral shift along the interface (see Fig. 4). For incidence below critical ($\theta < \theta_c$), $\not\angle n\,\Gamma$ is real and the lateral shift is complex; in this domain, it is physically more transparent to retain Γ as an amplitude as in Sec. IV A. It turns out that, <u>two</u> laterally shifted paths exist beyond critical incidence.

Pursuing the strategy outlined above for the n-th GB in the beam stacking scheme, we write (1) in the CSP form

$$I = -\frac{1}{4\pi i}\int_{-\infty}^{\infty}\frac{1}{\kappa_1(\xi)}\exp\{ik_1\Psi(\xi)\}d\xi \tag{6}$$

where

$$k_1\Psi(\xi) = \psi(\xi) - i\psi_r(\xi) \tag{6a}$$

$$\psi(\xi) = \xi(x-\tilde{x}_s) + \kappa_1(z+\tilde{z}_s) \tag{6b}$$

$$\psi_r(\xi) = \not\angle n\,\Gamma(\xi) \tag{6c}$$

Introducing a normalized spectral parameter

$$\tau = \frac{\xi}{k_1} \tag{7a}$$

and determining the saddle points τ_{nj} for $\theta > \theta_c$ from

$$\frac{d}{d\tau}\Psi(\tau_s) = (x-\tilde{x}_s) - \frac{\tau_s}{\sqrt{1-\tau_s^2}}(z+\tilde{z}_s) - \Delta = 0 \tag{7b}$$

where

$$\Delta = \frac{i}{k_1}\frac{1}{\Gamma}\frac{d\Gamma}{d\tau}\bigg|_{\tau=\tau_s} \tag{7c}$$

is the lateral shift, one obtains from the conventional saddle point technique [9] the asymptotic result

$$I_{ln} = -\frac{1}{4\pi i}\sum_j \left[\frac{-2\pi}{ik_1 \frac{d^2}{d\tau^2}\Psi(\tau_{nj})}\right]^{\frac{1}{2}} \frac{1}{\sqrt{1-\tau_{nj}^2}}\, e^{ik_1\Psi(\tau_{nj})} \tag{8}$$

here,

$$\Psi(\tau_{nj}) = \left[\tau(x-\tilde{x}_{ns}) + \sqrt{1-\tau^2}\,(z+\tilde{z}_{ns}) - i(n\,\Gamma(\tau)\right]_{\tau_{nj}} \tag{8a}$$

$$\left.\frac{d^2\Psi(\tau)}{d\tau^2}\right|_{\tau_{nj}} = -\frac{1}{(1-\tau^2)^{3/2}}(z+\tilde{\tau}_{ns})\Big|_{\tau_{nj}} - \frac{i}{k_1}\left[-\left(\frac{1}{\Gamma}\frac{d\Gamma}{d\tau}\right)^2 + \frac{1}{\Gamma}\frac{d^2\Gamma}{d\tau^2}\right]_{\tau_{nj}} \tag{8b}$$

In keeping with the beam shooting strategy that avoids solving the full saddle point condition in (7b) for a given observation point (x,z), we invoke the paraxial approximation. If

$$\xi_n^{(0)} = k_1 \sin\alpha_n \tag{9a}$$

is the saddle point for an observer located at (x_a,z_a) on the axis of the laterally shifted beam which is incident at the angle α_n, then the saddle point for an off-axis observer at (x,z) is

$$\xi = \xi_n^{(0)} + \delta \tag{9b}$$

The on-axis and off-axis observation points are related as follows

$$x = x_{an} + d_n \cos\alpha_n \ , \ z = z_{an} - d_n \sin\alpha_n \tag{9d}$$

and

$$d_n = r\sin(\theta - \alpha_n) - \Delta\cos\alpha_n$$

where r and θ are given by (4d). The paraxial expansion of the phase function $\Psi(\xi;x,z)$ in (6a) into power series about $(\xi_n^{(0)};x,z)$ involves up to quadratic terms in the parameters d_n and δ,

$$\Psi(\xi;x,z) \equiv \Psi(\xi_n^{(0)};x_{an},z_{an}) + \frac{\partial}{\partial d_n}\Psi(\xi_n^{(0)};x_{an},z_{an})\,d_n + \frac{\partial}{\partial\delta}\Psi(\xi_n^{(0)};x_{an},z_{an})\delta$$

$$+ \frac{1}{2}\left(d_n\frac{\partial}{\partial d_n} + \delta\frac{\partial}{\partial\delta}\right)^2 \Psi(\xi_n^{(0)};x_{an},z_{an}) \tag{10}$$

It is easily verified that

$$\frac{\partial}{\partial d_n}\Psi(\xi_n^{(0)};x_{an},z_{an}) = 0, \frac{\partial^2}{\partial d_n^2}\Psi(\xi_\alpha;x_a,z_a) \equiv 0 \tag{10a}$$

$$\frac{\partial}{\partial \delta}\Psi(\xi_n^{(0)};x_{an},z_{an}) = 0 \quad \text{(saddle point condition)} \tag{10b}$$

$$k_1\frac{\partial^2}{\partial d_n \partial \delta}\Psi(\xi_n^{(0)};x_{an},z_{an}) = \frac{1}{\cos\alpha_n} \tag{10c}$$

$$k_1\frac{\partial^2}{\partial \delta^2}\Psi(\xi_n^{(0)};x_{an},z_{an}) = -\frac{1}{k_1\cos^3\alpha_n}(z_{an} + \tilde{z}_{sn}) - i\frac{d^2\psi_r}{d\xi^2}\bigg|_{\xi_n^{(0)}} \tag{10d}$$

$$\frac{d^2}{d\xi^2}\psi_r(\xi) = -\left\{\frac{1}{\Gamma}\frac{d\Gamma}{d\xi}\right\}^2 + \frac{1}{\Gamma}\frac{d^2\Gamma}{d\xi^2} \tag{10e}$$

The saddle point equation in (10b) generally has two solutions, but only one of these turns out to be important for each beam element. Inserting the above expressions into (10) yields

$$k_1\Psi(\xi;x,z) = k_1\Psi(\xi_n^{(0)};x_{an},z_{an}) + \frac{1}{\cos\alpha_n}d_n\delta$$

$$-\frac{1}{2}\left[\frac{z_{an} + \tilde{z}_{sn}}{k_1\cos^3\alpha_n} + i\frac{d^2\psi_r(\xi_n^{(0)})}{d\xi^2}\right]\delta^2 \tag{11}$$

Since $\xi_n^{(0)} + \delta$ is the saddle point of the function $\Psi(\xi;x,z)$, it must satisfy the saddle point condition

$$k_1\frac{\partial}{\partial \delta}\Psi(\xi;x,z) = 0,$$

which furnishes the solution for δ,

$$\delta = \frac{d_n}{\cos\alpha}\left[\frac{z_{an}+\tilde{z}_{sn}}{k_1\cos^3\alpha_n} + i\frac{\partial^2\psi_r(\xi_n^{(0)})}{\partial\xi^2}\right]^{-1}. \tag{12}$$

Thus, from (11) and (12),

$$k_1\Psi(\xi;x,z) = k_1\Psi(\xi_n^{(0)};x_a,z_a) + \frac{1}{2}\left[\frac{z_{an}+\tilde{z}_{sn}}{k_1\cos^3\alpha_n} + i\frac{d^2\psi_r(\xi_n^{(0)})}{d\xi^2}\right]\delta^2 \tag{13}$$

or alternatively (see (7a) and (13))

$$k_1\Psi(\tau;x,z) = k_1\Psi(\tau_n;x,z) + \frac{1}{2}\frac{(k_1 d_n)^2}{k_1\tilde{R}_{an} + i\cos^2\alpha_n\dfrac{d^2\psi_r(\tau_n)}{d\tau^2}} \tag{14}$$

where $\tilde{R}_{an}$ is given in (4h), and

$$\frac{d^2\psi_r(\tau_n)}{d\tau^2} = \left[-\left(\frac{1}{\Gamma}\frac{d\Gamma}{d\tau}\right)^2 + \frac{1}{\Gamma}\frac{d^2\Gamma}{d\tau^2}\right]_{\tau_n}$$

Also

$$k_1\frac{d^2}{d\tau^2}\Psi(\tau_n;x,z) = -\left[k_1\tilde{R}_{an} + i\cos\alpha_n\frac{d^2\psi_r(\tau_n)}{d\tau^2}\right]\Big/\cos^2\alpha_n \tag{15}$$

Insertion of (14) and (15) into (8) completes the paraxial treatment of the laterally shifted beams for $\theta>\theta_c$. For $\theta<\theta_c$ one retains the PA-GB in (3b) with the approximations in (4a-c). The beam sum in (3) comprises all contributions (nonshifted for $\theta<\theta_c$ and shifted for $\theta>\theta_c$) that fit into the interval $\alpha^{(1)}<\alpha_n<\alpha^{(2)}$.

C. Reflected laterally shifted PA-GB plus head wave

This option is a hybrid combination of those in Secs. IVA and IVB, motivated by the observation that the laterally shifted ray incident near the critical angle does not account for the head wave as well as the branch point contribution in the non-shifted formulation, whereas the laterally shifted ray incident near the specular reflection angle has little effect on the head wave but does improve the totally reflected contribution (the reflection coefficient Γ is not necessarily slowly varying (i.e. an amplitude function) for strongly oblique incidence). As before, incident ray fields ahead of and near the critical angle are modeled by PA-GB.

The GB implementation of the integral (1) here was initially structured as follows. The observational domain $0 \leq \theta < \frac{\pi}{2}$ was divided into three subintervals: $1: 0 \leq \theta < \theta_1$; $2: \theta_1 \leq \theta < \theta_2$; $3: \theta_2 \leq \theta < \frac{\pi}{2}$. In interval 1, the nonshifted PA-GB alone were used, in interval 2, the PA-GB were augmented by the (asymptotically approximated) head wave, while interval 3 was covered by the laterally shifted PA-GB as in (8) plus the (asymptotically approximated) head wave. Accordingly,

$$I_n = \begin{cases} I_{sn}\ , & \theta \leq \theta < \theta_1 \quad (16a) \\ I_{sn} + I_{bn}\ , & \theta_1 \leq \theta < \theta_2 \quad (16b) \\ I_{ln} + I_{bn}\ , & \theta_2 \leq \theta < \frac{\pi}{2} \quad (16c) \end{cases}$$

where I_{sn} and I_{bn} are given by (3b) and (5b), respectively, while I_{ln} is given by (8). The angle $\theta_1 > \theta_c$ corresponds to a numerical $|ND| \approx 2$, whereas the angle $\theta_2 > \theta_c$ corresponds to a numerical distance $|ND| > 2$ which is problem dependent. From numerical experience for various ranges of medium parameters and source locations, we chose $\theta_2 \approx 1.02\theta_c$.

The choice of the three intervals above was regarded to be in accord with the phenomenological spirit of the hybrid formulation. Nonshifted PA-GB plus branch point asymptotics can account for phenomena near the critical angle because the branch point (head wave) and saddle point (reflected beam) in the spectral integrand are so close to one another that the spectral coverage of both overlaps. As θ increases away from θ_c, the two contributions become distinct and are known to be poorly accomodated by narrow nonshifted PA-GB. This deficiency is to be overcome by the laterally shifted reflected PA-GB for $\theta > \theta_2$, where θ_2 is only loosely defined. When this scenario was implemented numerically, tests were run as well wherein the interval 2 in (16b) was eliminated, and interval 3 in (16c) extended from $\theta_1 \leq \theta \leq \pi/2$. The results obtained so far were practically unchanged, thereby indicating that for the problem parameters explored here, the laterally shifted PA-GB, which accounts essentially for specular reflection away from the critical angle can be safely extended up to the $|ND| = 2$ limit. This simplifies the algorithm, which thus comprises (16a) and (16c), with θ_1 corresponding to $|ND| = 2$.

V. Numerical Results

Extensive numerical results have been generated for the analytical models in Secs. III and IV, when applied to typical elastic rock interface or to ocean-(fluid-bottom) environments. Selected sets of data are shown in Fig. 5, with primary emphasis on how the results are affected by the choice of beam widths in the Gaussian stack. The half-width w_0 of the beam waist at a level where the amplitude equals (1/e) = 1/2.71828 times the maximum amplitude, is related to the beam parameter b, which

measures the Fresnel distance corresponding to w_0, as follows:

$$b = \pi w_0^2/\lambda_1 \tag{17}$$

where λ_1 is the wavelength in the source medium 1. The angular spacing $\Delta\alpha$ between beams, for specified w_0 or b, is such that adjacent beams overlap at their (1/e) amplitude points. The total number of beams in the stack is determined by any one of the following three criteria: a) $|\theta - \alpha_N| \geq \pi/2$, where α_n is the beam axis angle and θ is the angle of the ray that connects source and observer (the n=0 beam has angle $\alpha_0 = \theta$); b) (amplitude of beam with α_{N+1}) $\leq (10^{-4}$ times n = 0 to N beam sum); c) $\alpha_N \geq \pi/2$. Note that N may be different for $\alpha_n < \theta (N = N_1)$ and $\alpha_n > \theta (N = N_2)$, so that the total number of beams is $N_1 + N_2 + 1$). Each beam is treated by the CSP method, which involves the complex image point $(\tilde{x}_{sn}, -\tilde{z}_{sn})$, with $\tilde{x}_{sn} = x_{sn} + b\sin\alpha_n$, $\tilde{z}_{sn} = z_{sn} + ib\cos\alpha_n$ (this is a convenience, not a restriction; alternatively, the beams could have been tracked from the source to the observer via the interface); here, (x_{sn}, z_{sn}) locates the n-th beam waist center. Other relevant quantities have been defined in (3e).

We recall that in the PA-GB option, the beams alone (either via the conventional or the improved PA) are included (see (3) and (4)). In the PA-GB plus head wave option, the PA-GB are included as above (see (3) and (4)), and the head wave in (5b) is added to the n-th beam when each of the following two criteria is satisfied: a) $\theta > \theta_c$, where θ_c is the critical angle; b) $(ND)_n \geq 2.0$, where $(ND)_n$ is the numerical distance in (5f). While $(ND)_n \geq 2$ has been found safe for validity of branch point asymptotics over a broad parameter range, one may "tune up" the restriction to lower ND values by numerical experiment in specific cases.

When the beam parameter b is larger than 50 λ_1, the numerical results become unstable and indicate that the angular interval $\Delta\alpha$ must be reduced below the (1/e) overlap criterion by the addition of more beams. The difficulty is caused by the increasingly rapid variation of the phase term $ik_1\tilde{R}_n$ in (3b) with α_n, as b increases. For example, when $500\lambda_1 \leq b \leq 1000\lambda_1$, it has been found that $\Delta\alpha \approx 0.004$ is needed for stability whereas the 1/e overlap criteria gives $\Delta\alpha \approx 0.0178$. It may also be noted that the laterally shifted beams near the critical angle require tighter sampling than the nonshifted PA-GB. Again, when $500\lambda_1 < b < 1000\lambda_1$, stability sets in when $\Delta\alpha \approx 0.00178$. As before, the difficulty arises from the very rapidly fluctuating phase when the reflection coefficient, which varies rapidly near the critical angle, is incorporated into the phase. The sensitive regions are near the critical angle and near the zero reflection (Brewster) angle (when that exists); when sampling, is the synthesized results are not smooth in these regions.

Addressing the above difficulties by increasing the number of beams led to the parameters listed below. For the conventional nonshifted PA-GB, the beam stacking interval was determined as follows:

$$\Delta\alpha = 0.2\left[\frac{\lambda_1}{\pi b}\right]^{1/2}, \qquad 50\lambda_1 < b < 500\lambda_1 \tag{17a}$$

$$\Delta\alpha = 0.15\left[\frac{\lambda_1}{\pi b}\right]^{1/2}, \qquad 500\lambda_1 \le b \le 5000\lambda_1 \tag{17b}$$

The corresponding number of beams is

$$\begin{cases} b = 100\lambda_1 (w_0 = 5.6\lambda_1), N_1 + N_2 \approx 50 \\ b = 1000\lambda_1 (w_0 = 17.8\lambda_1), N_1 + N_2 \approx 130 \\ b = 5000\lambda_1 (w_0 = 39.9\lambda_1), N_1 + N_2 \approx 580 \end{cases} \tag{18}$$

For the nonshifted PA-GB plus head wave option, $\Delta\alpha$ and $N_1 + N_2$ are the same as above. For the hybrid option, more beams are required for numerical stability. By numerical tests, we chose

$$\Delta\alpha = 0.06\left[\frac{\lambda_1}{\pi b}\right]^{1/2}, \qquad b < 1000\lambda_1 \tag{19a}$$

$$\Delta\alpha = 0.04\left[\frac{\lambda_1}{\pi b}\right]^{1/2}, \qquad 1000\lambda_1 \le b \le 5000\lambda_1 \tag{19b}$$

with the corresponding number of beams

$$\begin{cases} b = 100\lambda_1, \ N_1 + N_2 \approx 280 \\ b = 1000\lambda_1, \ N_1 + N_2 \approx 890 \\ b = 5000\lambda_1, \ N_1 + N_2 \approx 980 \end{cases} \tag{20}$$

Truncation of the beam stacks according to the criteria listed after (17) must be performed with care when the bottom medium allows for Brewster angle effects where the plane wave reflection coefficient vanishes. Although the reflected beams very near the Brewster angle $\theta = \theta_b$ make a negligible contribution at the observation point, the beam stack may be truncated there only when these contributions remain negligible in a large enough neighborhood of θ_b. We have found that such a

neighborhood is adequately defined by $\theta_b \pm \Delta$, where $\Delta \approx 0.01\theta_b$.

For the laterally shifted PA-GB option in Section IVB, similar caution must be exercised concerning truncation. The laterally shifted PA-GB stack yields strongly contributing clusters near the critical angle θ_c and near the specular reflection angle θ. Truncation of the total beam stack by applying the above-cited criteria can lead to the exclusion of the other cluster. Therefore, no truncation should be undertaken in the angular interval between θ_c and θ.

References

1. V. Cerveny, "Gaussian Beam Synthetic Seismograms," J. Geophys. Res., 58, 44-72 (1985).

2. R. Nowack and K. Aki, "2-D Gaussian Beam Synthetic Method: Testing and Application," J. Geophys. Res., 89, 1466-1494, (1984).

3. J. Konopaskova, and V. Cerveny, "Numerical Modelling of Time Harmonic Seismic Wave Fields in Simple Structures." Part I: Studia geophys. geod., 28, 19-35. Part II Studia geophys. geod., 28, 113-128.(1984)

4. L.M. Brekhovskikh, Waves In Layered Media, Acad. Press, New York, sec. ed., sec. 30 (1980).

5. I. Tai Lu, L.B. Felsen, and Y.Z. Ruan, "Spectral Aspects of the Gaussian Beam Method: Reflection from a Homogeneous Half Space," Geophys. J.R. astr. Soc., 89, 915-932 (1987).

6. L.B. Felsen, "Geometrical Theory of Diffraction, Evanescent Waves, Complex Rays and Gaussian Beams," Geophys. J.R. Astr. Soc., 79, 77-88 (1984).

7. J.W. Ra, H.L. Bertoni and L.B. Felsen, "Reflection and Transmission of Beams at a Dielectric Interface," SIAM J. Appl. Math., 24, 396-413 (1973).

8. X.J. Gao, and L.B. Felsen, "Complex Ray Analysis of Beam Transmission Through Two-Dimensional Radomes," IEEE Trans. Antennas and Propag., AP-33, 967-975 (1985).

9. L.B. Felsen, and N. Marcuvitz, Radiation and Scattering of Waves, Prentice-Hall, New Jersey, Chapter 4 (1973).

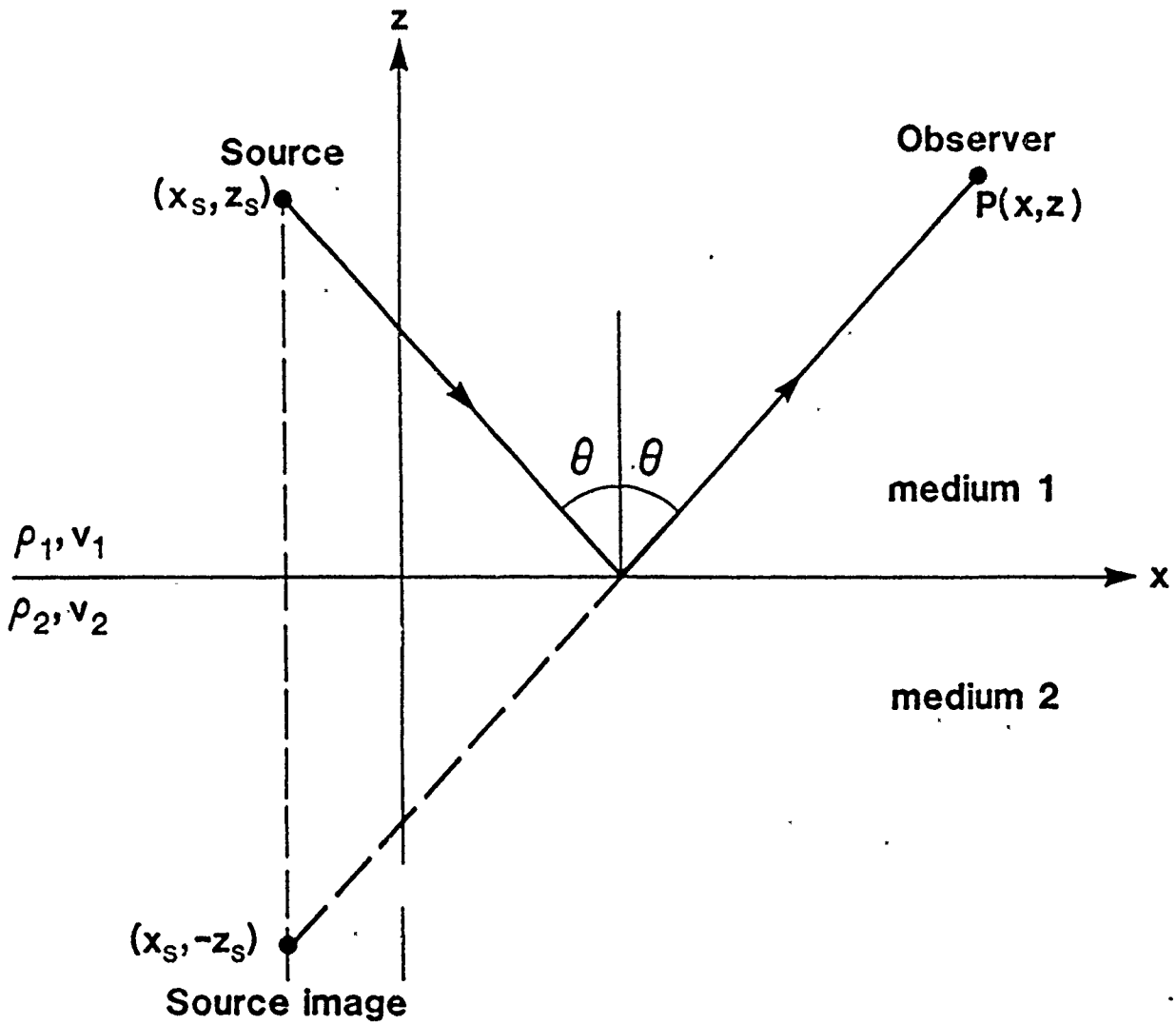

Fig. 1 Physical configuration of line-source-excited half space with interface at z=0

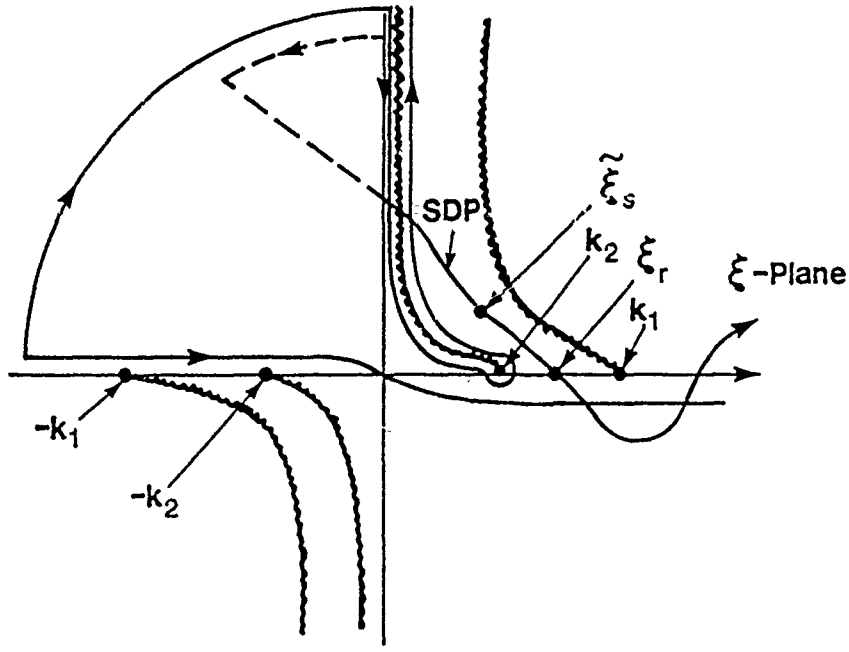

(a) Complex ξ-Plane

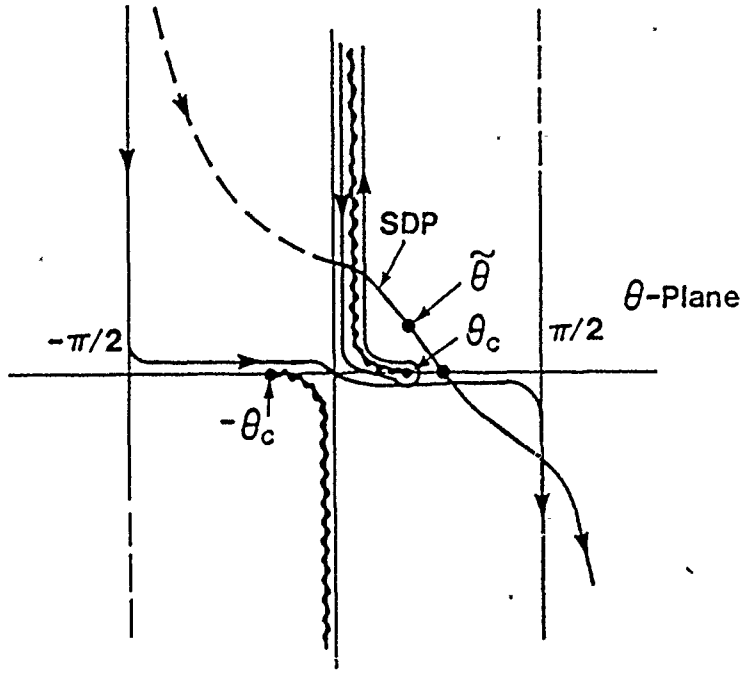

(b) Complex θ-plane

Fig. 2. Integration contours in complex spectrum planes

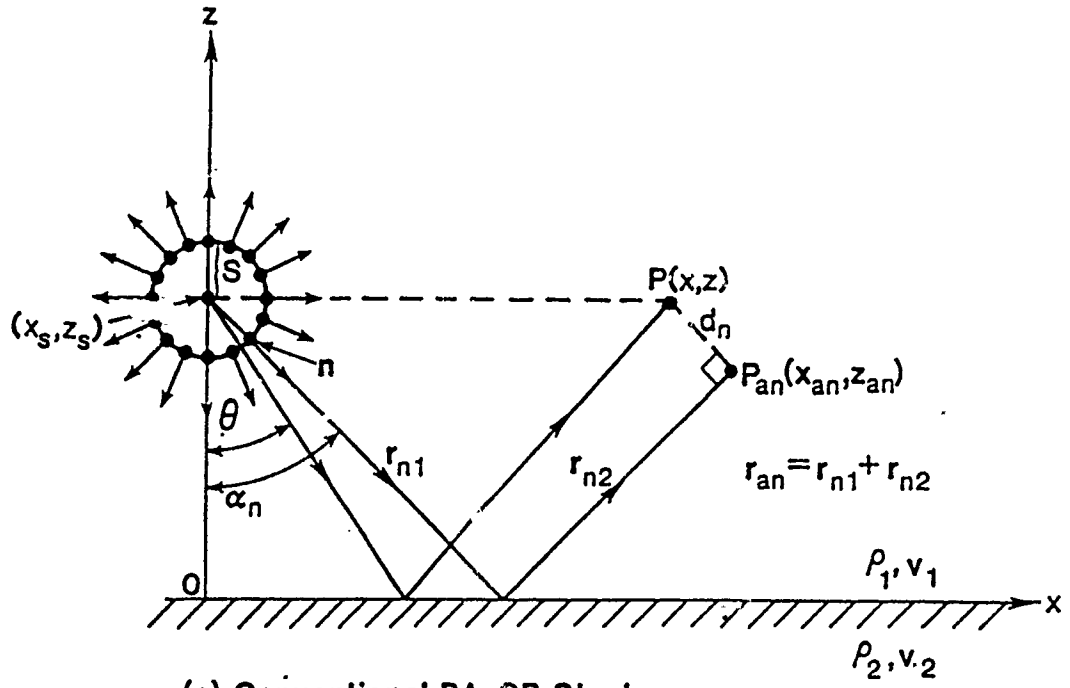

(a) Conventional PA-GB Stack.

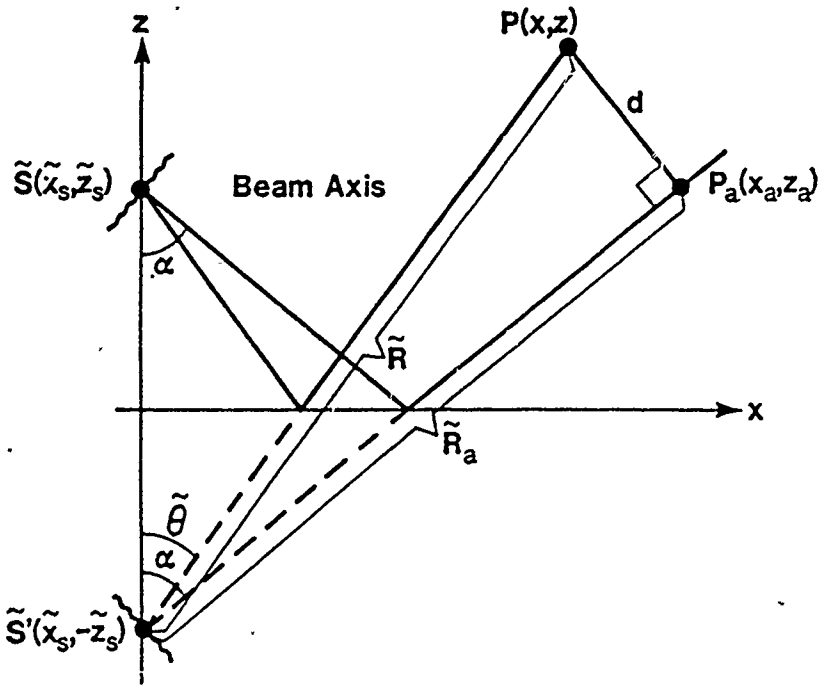

(b) Conventional and the full CSP PA-GB.

Fig. 3 Beam Parameters for Line-Source-Excited Reflection.

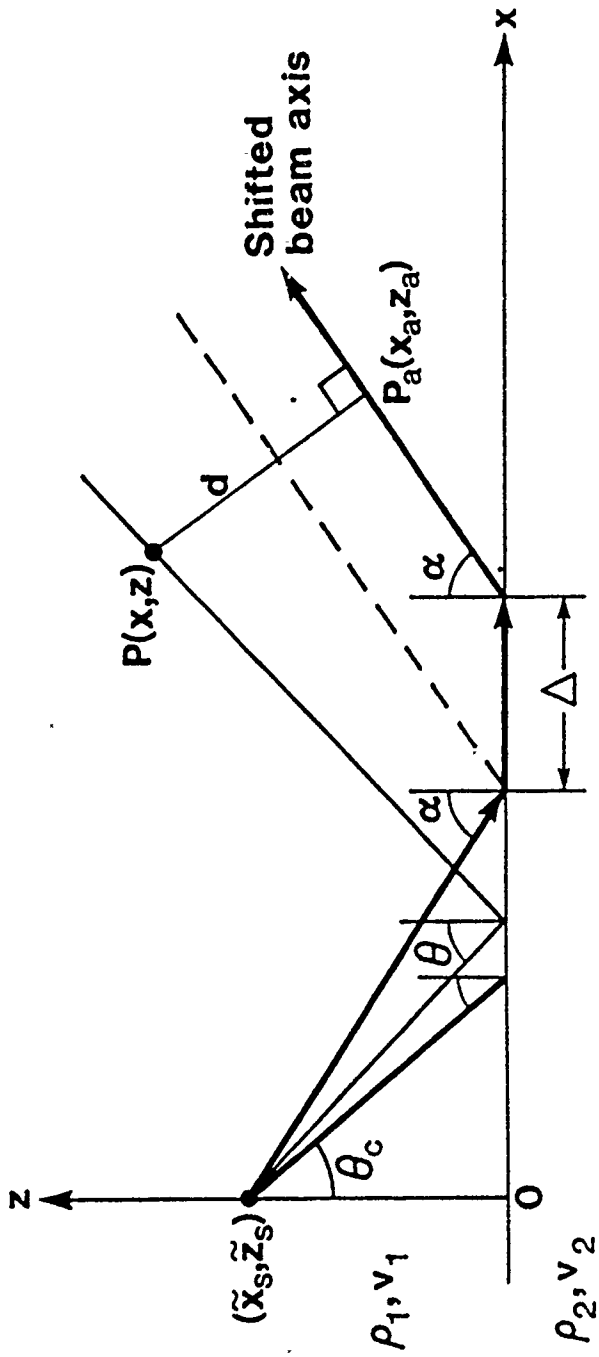

Fig. 4 Parameters pertaining to the laterally shifted PA-GB.

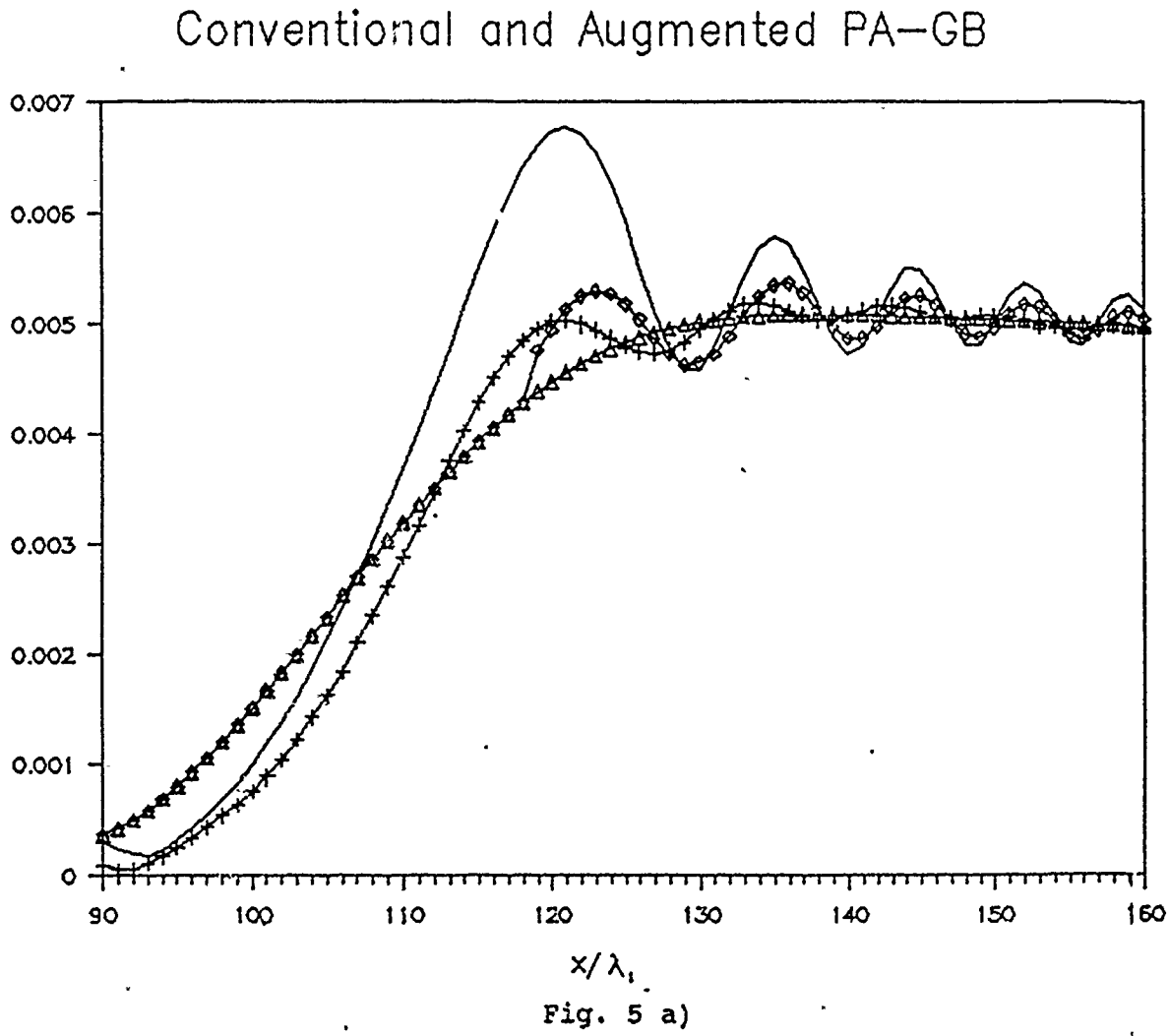

Fig. 5. SH field synthesis by conventional PA-GB and its augumented options for line source in the presence of a plane interface separating two elastic half spaces

Parameters:

frequency $f = 1$ hz
wave length in medium 1 $\lambda_1 = 1$
density ρ_1 = density $\rho_2 = 1$
$v_1 = D_1$/sec
$v_2 = 2.1523 v_1$
critical angle: $\theta_c = 27.6$ Degs. ($x = 104.3\,\lambda_1$)
observation plane: $z = 100\,\lambda_1$
line source location: $z_s = 0, z_o = 100\lambda_1$
numerical distance ND = 2

Legend:

—— : Reference solution
△ : PA-GB only
◇ : PA-GB plus head wave
\+ : PA-GB with lateral shift

(a) $b = 100\,\lambda_1$ ($w_0 = 5.6\lambda_1$)
(b) $b = 200\,\lambda_1$ ($w_0 = 7.98\lambda_1$)
(c) $b = 500\,\lambda_1$ ($w_0 = 12.6\lambda_1$)
(d) $b = 1000\,\lambda_1$ ($w_0 = 17.8\lambda_1$)
(e) $b = 2000\,\lambda_1$ ($w_0 = 25.2\lambda_1$)
(f) $b = 5000\,\lambda_1$ ($w_0 = 39.9\lambda_1$)

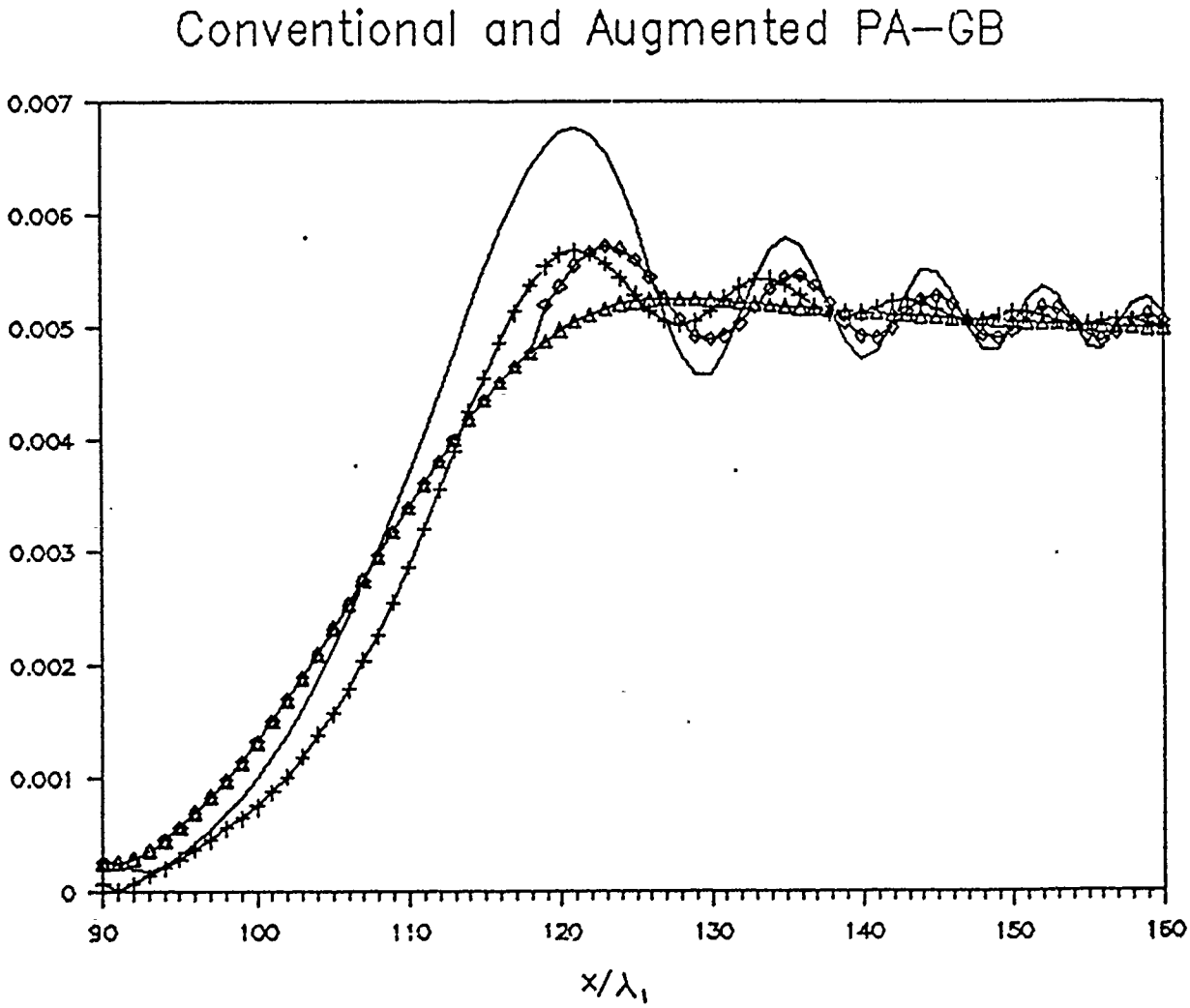
Conventional and Augmented PA—GB
0.007
0.006
0.005
0.004
0.003
0.002
0.001
0
90
100
110
120
130
140
150
160
x/λ1

Fig. 5 b)

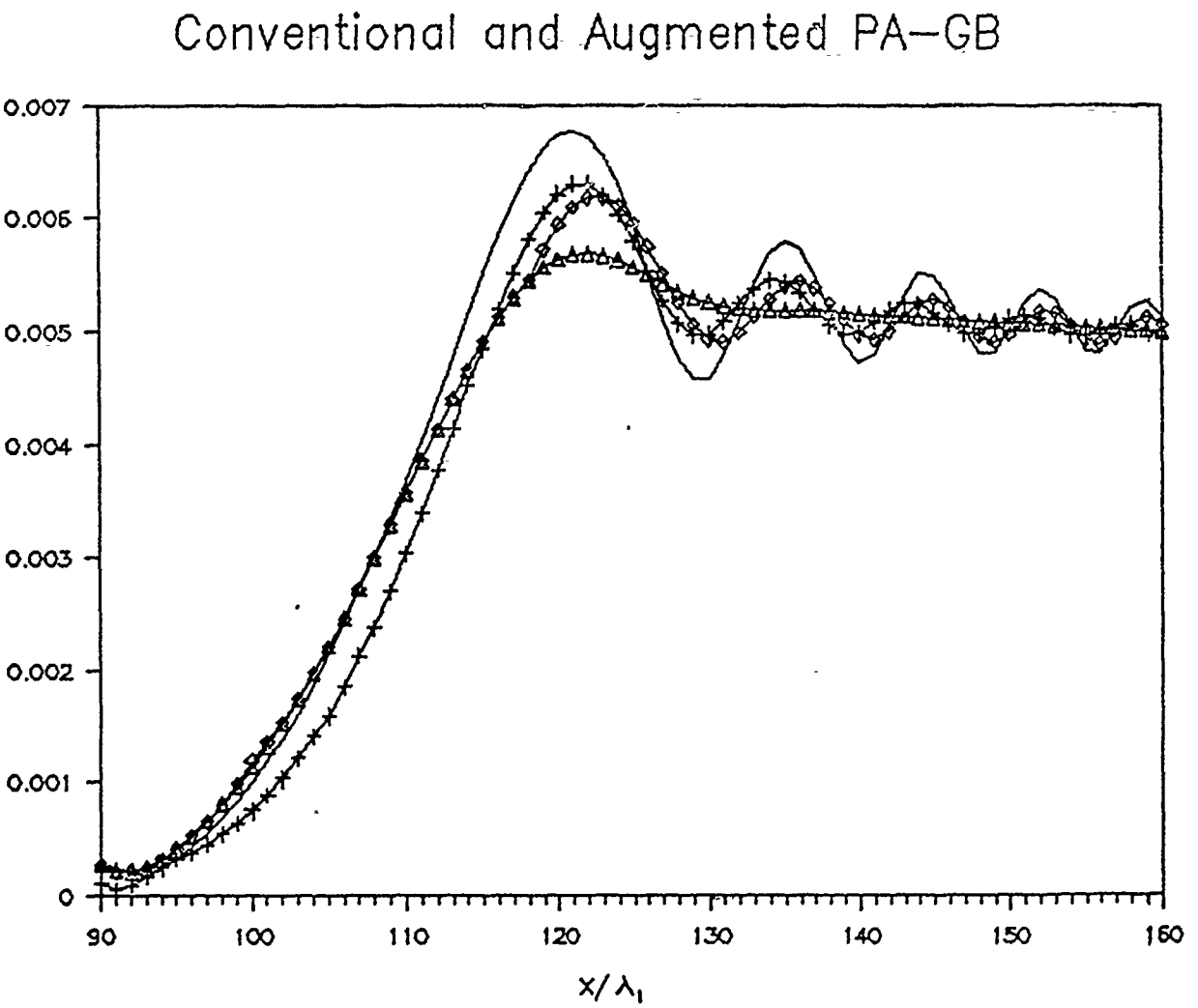
Conventional and Augmented PA–GB
0.007
0.006
0.005
0.004
0.003
0.002
0.001
0
90
100
110
120
130
140
150
160
X/λ1

Fig. 5 c)

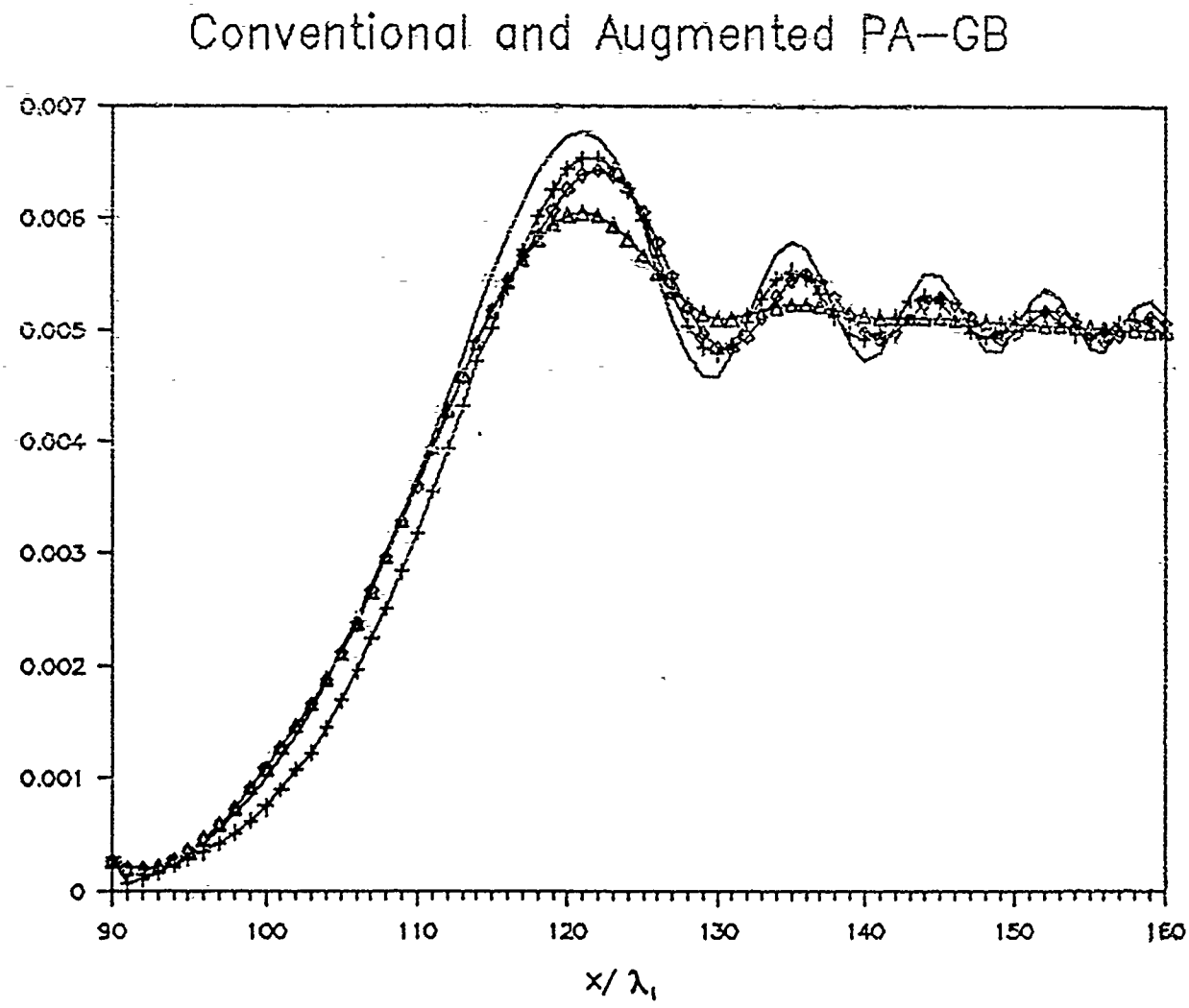
Conventional and Augmented PA–GB
0.007
0.006
0.005
0.004
0.003
0.002
0.001
0
90
100
110
120
130
140
150
160
x/ λ1

Fig. 5 d)

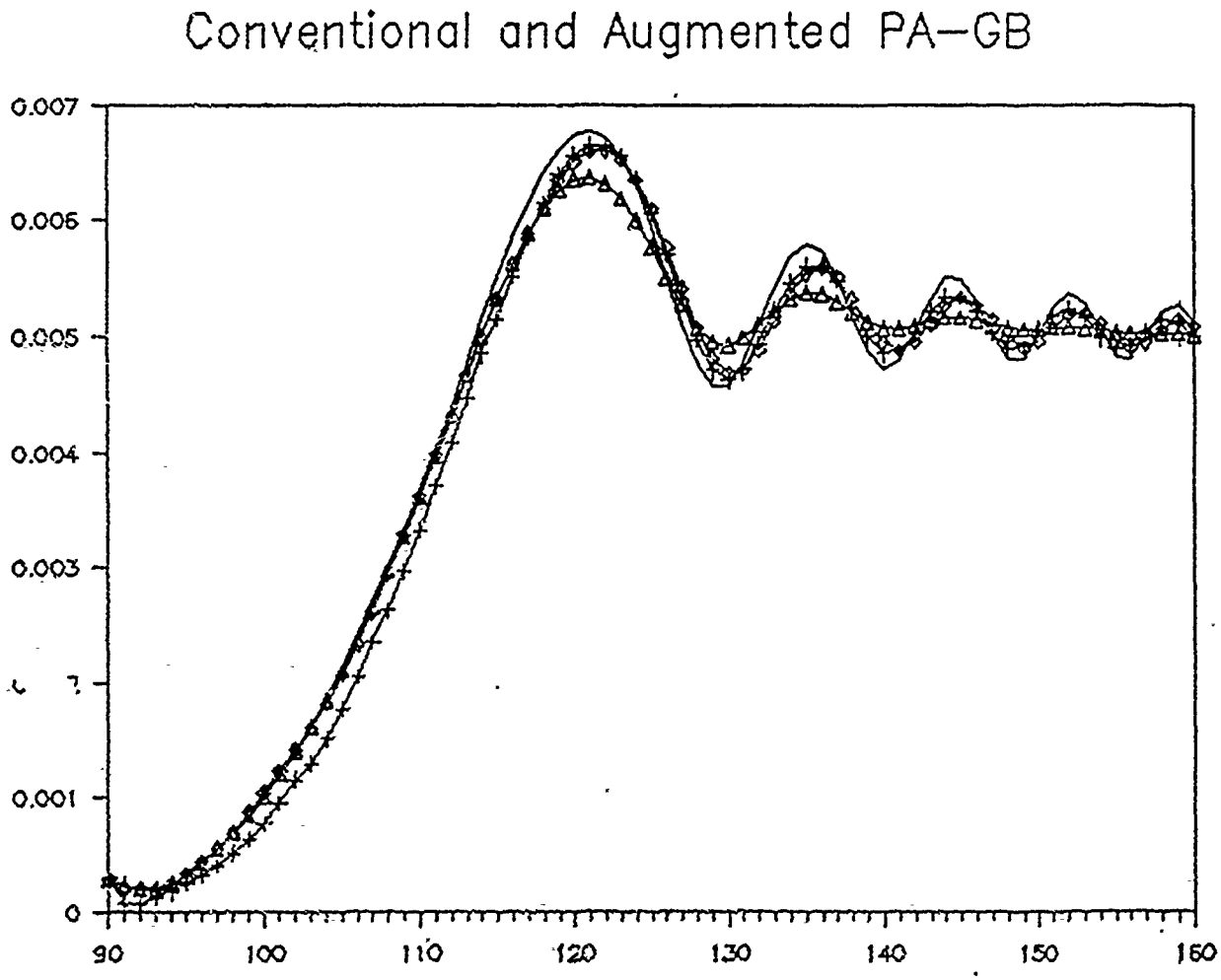
Conventional and Augmented PA–GB
0.007
0.006
0.005
0.004
0.003
0.001
0
90
100
110
120
130
140
150
160
x/ λ1

Fig. 5 e)

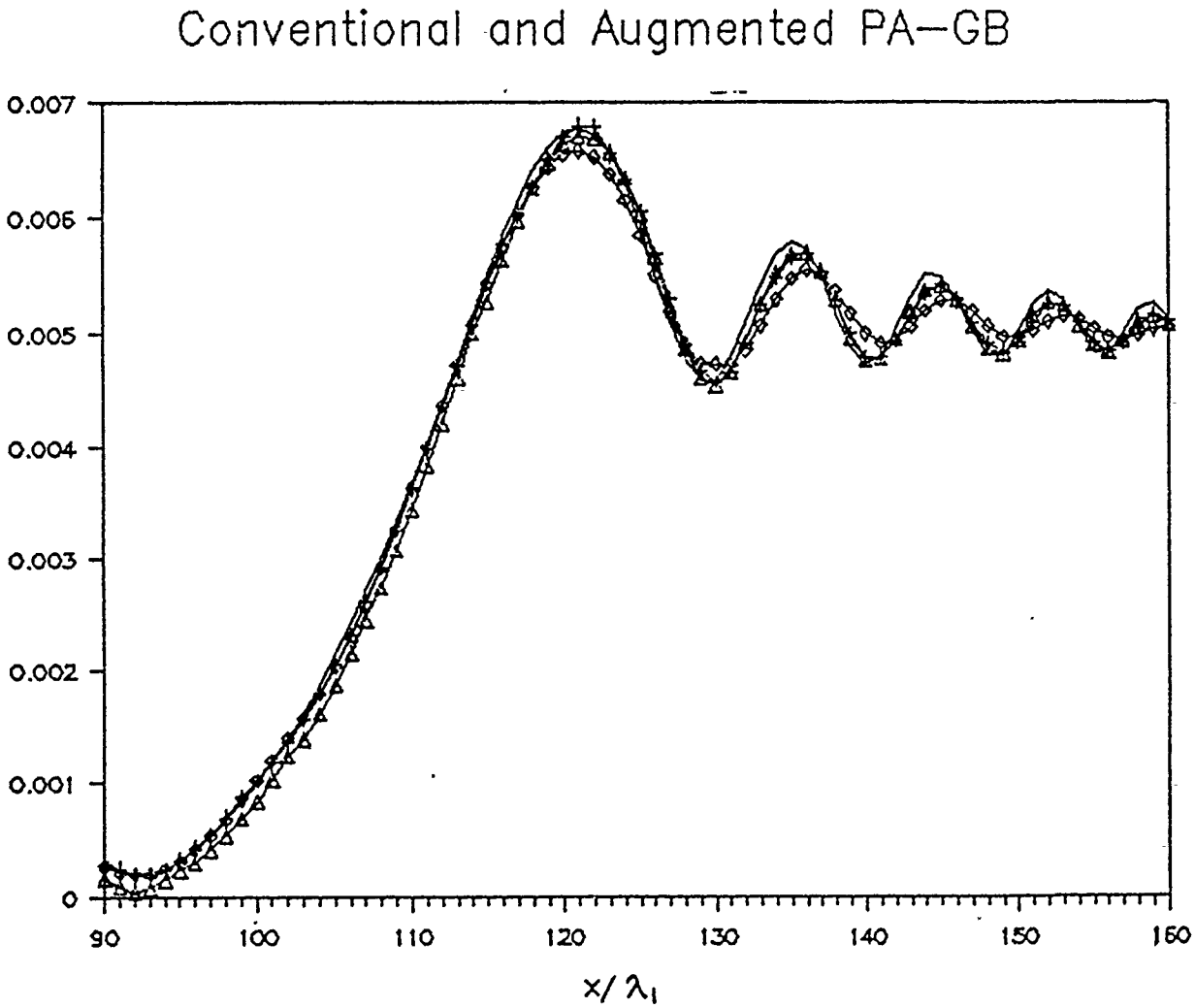
Conventional and Augmented PA—GB
0.007
0.006
0.005
0.004
0.003
0.002
0.001
0
90
100
110
120
130
140
150
160
x/λ1

Fig. 5 f)

Section III

Hybrid Ray-Mode Formulation of High Frequency Propagation in a Bilinear Tropospheric Surface Duct

Hybrid Ray-Mode Formulation of High Frequency Propagation in a Bilinear Tropospheric Surface Duct

T. Ishihara and L.B. Felsen

I. Introduction

Analytical modeling of wave propagation in the earth's environment poses formidable problems because of the complexity of the propagation channel. The troposphere, which provides such a channel for electromagnetic waves, can generally be described by a permittivity $\epsilon(\underline{r})$ that varies vertically as well as laterally with respect to the earth's surface. Of special interest are conditions where the vertical profile of $\epsilon(\underline{r})$ is such as to permit wave ducting adjacent to the earth's surface or at moderate heights, with lateral variations occurring on a scale that is gradual compared with those in height. Because the problem scale is large at high frequencies and for long propagation distances, direct numerical modeling is either inefficient or not feasible. Therefore, an effective algorithm must be parametrized in terms of wave objects that can negotiate long range propagation. Possible choices include ray fields, mode fields, parabolic propagators, beams, etc., either for single species models or, more effectively, in hybrid combinations that seek to take advantage of the most favorable features of each. The analytical models must be self-consistent approximations of the intractable rigorously formulated problem. To ascertain their accuracy, they must be tested on tractable simpler canonical environments that allow generation of numerical reference solutions. Moreover, the test environments should be such as to deviate only weakly from the realistic environment, thereby validating analytic techniques of adiabatic adaptability of each wave object from the test problem to the realistic case without, or with only weak, coupling to other wave objects.

The present study seeks to apply these concepts to high frequency electromagnetic wave propagation in a tropospheric surface or elevated duct, initially without, and eventually with, lateral inhomogeneities. In the test environment, the permittivity is assumed to depend on height only, and the earth's influence is modeled by a constant surface impedance, thereby rendering the propagation problem separable in a spherical coordinate system. Because the (vertical electric dipole) source and observer locations of interest are at levels above the earth which are small compared to the earth's radius, it is possible to invoke approximations that map the spherical geometry into an equivalent rectangular geometry. A normalized field solution, usually referred to as the attenuation function, is then obtained in a spectral integral form that serves as the starting point for developing desirable parametrizations. The

considerations pertaining to this strategy have been well documented in the technical literature [], and they are summarized in Sections II and III. In Section IV, detailed consideration is given to a bilinear permittivity profile which has also received much attention from other investigators []. After deriving the spectral integral solution for that special case (Section IV.A), alternative solutions are developed in the form of an expansion over normal (guided) modes propagating parallel to the earth's surface (Section IV.B), a ray field expansion (Section IV.C), and a hybrid ray-mode expansion that combines ray fields and mode fields self-consistently (Section IV.D).

II. Formulation

Adopting a spherical $\underset{\sim}{r}=(r,\theta,\phi)$ coordinate system, we consider wave propagation due to a vertical electric dipole located near the earth's surface in a radially varying troposphere modeled by a permittivity $\epsilon(r)$. The electrical properties on the earth's surface at $r=a$ are assumed to be specified by a surface impedance Z_s. In view of the environmental dependence on r only, the radial dipole source excites fields that are azimuthally independent about its axis. If the polar axis of the spherical coordinate system is chosen to pass through the source at $r=r'$, the magnetic and electric fields are specified in that system by the components H_ϕ and E_r, E_θ, respectively (Fig. 1). All field components can be derived from a scalar potential $U(\underset{\sim}{r})=U(r,\theta)$ via the relations [1,2]

$$E_r = \frac{-1}{r\sin\theta}\frac{\partial}{\partial\theta}\sin\theta\frac{\partial U}{\partial\theta} \tag{1}$$

$$E_\theta = \frac{1}{\epsilon(r)r}\frac{\partial}{\partial r}\left[\epsilon(r)r\frac{\partial U}{\partial\theta}\right] \tag{2}$$

$$H_\phi = i\omega\epsilon(r)\frac{\partial U}{\partial\theta} \tag{3}$$

with $U(r)$ determined from the scalar wave equation

$$\frac{\partial}{\partial r}\frac{1}{\epsilon(r)}\frac{\partial}{\partial r}[\epsilon(r)(rU)] + \frac{1}{r\sin\theta}\frac{\partial}{\partial\theta}\sin\theta\frac{\partial}{\partial\theta}U + k^2(r)r(U) = 0 \tag{4}$$

$$k^2(r) = \omega^2\epsilon(r)\mu_o = \omega^2\epsilon_o\mu_o\epsilon_s(r) = k_o^2\epsilon_s(r) \tag{4a}$$

In (4a), $\epsilon_s(r)$ is the permittivity normalized with respect to the permittivity ϵ_o in vacuum, and k_o is the wavenumber in vacuum. All field quantities have a suppressed time dependence $\exp(-i\omega t)$. The impedance boundary condition

$$E_\theta = -Z_s H_\phi \tag{5}$$

implies that

$$\frac{1}{\epsilon(r)r}\frac{\partial}{\partial r}[\epsilon(r)rU] = i\omega\epsilon(r)Z_s U \qquad \text{on } r=a \tag{6}$$

At $|r| \to \infty$, the potential must satisfy the radiation condition.

Because the radial locations of the source and observation points satisfy the inequalities $(r'/a) \ll 1$, $(r/a) \ll 1$, the exact equation in (4) can be approximated. By a sequence of scalings and redefinitions of coordinates, one may transform the field dependence from the spherical (r,θ) coordinates into an equivalent dependence in rectangular (y,x) coordinates [1,2]. The approximate source-excited transformed wave equation becomes

$$\left[\frac{\partial^2}{\partial y^2} + i\frac{\partial}{\partial x} + p(y)\right]\psi(x,y) = -\delta(x)\delta(y-y') \tag{7}$$

subject to the boundary condition

$$\frac{\partial}{\partial y}\psi + q\psi = 0 \quad \text{at } y=0 \tag{7a}$$

and a radiation condition at infinity. The following definitions have been utilized:

$$x = m\theta, \quad y = \frac{k}{m}(r-a), \quad y' = \frac{k}{m}(r'-a) \quad , \tag{8a}$$

$$k = k(0), \quad m = \left(\frac{ka}{2}\right)^{1/3}, \quad q = \text{im}[\epsilon_s(0)]^{1/2}Z_s/Z_o \tag{8b}$$

The "attenuation function" ψ is derived from the normalized potential

$$U/U_o = 2(\pi x)^{1/2}\, e^{i\pi/4}\, \psi \ , \tag{9}$$

where U_o is the potential for the same dipole located in the presence of a plane perfectly conducting earth. Because this normalization extracts the "strong"

phase variation along $\theta \rightarrow (x/m)$, one obtains the simplified parabolic equation in (7). The equivalent permittivity function p(y) is given by

$$p(y) = y + \gamma(y), \quad \gamma(y) = m^2 \left[\frac{\bar{\epsilon}_s(y)}{\bar{\epsilon}_s(0)} - 1 \right], \quad \bar{\epsilon}_s(y) \equiv \epsilon_s(a + my/k) \qquad (10)$$

This completes the formulation of the problem.

III. Spectral Integral Solution

The reduced eqution in (7) for the attenuation function is separable in the (x,y) coordinates. The most general form of the solution, from which various alternative representations can be derived, is built around a complex wavenumber spectrum. Introducing a complex spectral variable (separation parameter) t (this parameter should not be confused with the deleted time dependence $\exp(-i\omega t)$), and recognizing that the $(\partial/\partial x)$ operator is algebraized by an exponential function $\exp(ixt)$ so that $(i\partial/\partial x) \rightarrow -t$, one obtains for the y-dependent spectrum the one-dimensional Green's function problem,

$$\left\{ \frac{d^2}{dy^2} + [p(y) - t] \right\} g_y(y,y';t) = -\delta(y-y') \quad , \qquad (11)$$

which has the solution []

$$g_y(y,y';t) = \frac{[f_2(y_<,t) + R_o f_1(y_<,t)] f_1(y_>,t)}{W[f_1,f_2]} \qquad (12)$$

where the Wronskian W is given by

$$W[f_1,f_2] = f_1 f_2' - f_1' f_2 \quad , \quad f' \equiv df/dt \qquad (12a)$$

and the reflection coefficient R_o by

$$R_o = - \frac{f_2'(0,t) + q f_2(0,t)}{f_1'(0,t) + q f_1(0,t)} \qquad (12b)$$

In (12), f_1 and f_2 are linearly independent solutions of the source-free equation in (11), which are employed in the combination shown to satisfy the boundary conditions at $y = 0$ and $y \rightarrow \infty$, respectively, while $y_<$ and $y_>$ denote the smaller or larger values of y and y', respectively. Spectral synthesis then yields the following solution,

$$\psi = \frac{1}{-2\pi i} \oint e^{ixt} g_y(y,y';t)\,dt \tag{13}$$

This result furnishes the starting point for the detailed studies that follow.

IV. Bilinear Permittivity Profile

A. Spectral integral

We shall consider for the equivalent permittivity p(y) in (10) the bilinear profile (Fig. 2)

$$\gamma(y) = (1+\mu^3)(y_i - y) \quad \text{for} \quad 0 < y \leq y_i \tag{14a}$$

$$\gamma(y) = 0 \quad \text{for} \quad y_i \leq y \tag{14b}$$

where μ is a parameter to be determined from the profile expressed in the original (r,θ) coordinates. In (14), for subsequent convenience, the reference permittivity has been placed at $y=y_i$; accordingly, the reference permittivity $\bar{\epsilon}_s(0)$ in (10) should be replaced by $\bar{\epsilon}_s(y_i)$. If we write

$$\frac{\bar{\epsilon}_s(y)}{\bar{\epsilon}_s(y_i)} = 1 - b_o \frac{m}{k}(y - y_i) \quad , \quad y < y_i \tag{15}$$

then the profile parameters in (15) and (14) are related via

$$\mu = \left(\frac{ab_o}{2} - 1\right)^{1/3} \tag{16}$$

To reduce the equation in (11), with (14), to a standard form, we introduce the scaled coordinate and spectral variables ξ and τ,

$$\xi = \tau + \mu y \,, \quad \tau = [t - (1+\mu^3)y_i]/\mu^2 = \left(t - \frac{ab_o y_i}{2}\right)/\mu^2 \tag{17}$$

from which

$$\mu^2 \xi_i = t - y_i \tag{17a}$$

where $\xi=\xi_i$ corresponds to $y=y_i$. Then the generic equation for the source-free solutions $f=f_{1,2}$ in (12) becomes the Airy equation

$$\frac{d^2}{d\xi^2}f - \xi f = 0 \qquad \tau < \xi < \xi_i \tag{18}$$

Accordingly, the spectral integral in (13) may be written explicitly in terms of the Airy functions Ai, Bi,

$$\psi(x,y) = \frac{1}{2\mu i}\int_{-\infty}^{\infty} \frac{\tilde{f}(y_<,t)\tilde{f}(y_>,t)}{1-R_o(t)R_i(t)}\, e^{ixt}dt \tag{19}$$

where

$$\tilde{f}(y_<,t) = Ai(\tau+\mu y_<) + R_o Bi(\tau+\mu y_<) \tag{19a}$$

$$\tilde{f}(y_>,t) = Bi(\tau+\mu y_>) + R_i Ai(\tau+\mu y_>) \tag{19b}$$

with the spectral reflection coefficients R_o and R_i that arise from the earth's surface at $y=0$ and the profile slope discontinuity at $y=y_i$, respectively,

$$R_o = -\frac{\mu Ai'(\tau)+qAi(\tau)}{\mu Bi'(\tau)+qBi(\tau)} \tag{19c}$$

$$R_i = \frac{\mu Bi'(\tau+\mu y_i)+\dfrac{w_i'(t-y_i)}{w_i(t-y_i)}Bi(\tau+\mu y_i)}{\mu Ai'(\tau+\mu y_i)+\dfrac{w_i'(t-y_i)}{w_i(t-y_i)}Ai(\tau+\mu y_i)} \tag{19d}$$

Alternative representations with different convergence properties will now be derived from the spectral continuum in (19).

B. Normal Mode Expansion

The integrand in (19) has pole singularities t_m at the zeros of the denominator (the index m here is not to be confused with the parameter m in (8b)),

$$1 - R_o(t_m)R_i(t_m) = 0\ , \qquad m = 1,2,3,--- \tag{20}$$

or explicitly

$$\frac{\mu Ai'(\tau_m)+qAi(\tau_m)}{\mu Bi'(\tau_m)+qBi(\tau_m)} = \frac{\mu w_i(t_m-y_i)Ai'(\tau_m+\mu y_i)+w_i'(t_m-y_i)Ai(\tau_m+\mu y_i)}{\mu w_i(t_m-y_i)Bi'(\tau_m+\mu y_i)+w_i'(t_m-y_i)Bi(\tau_m+\mu y_i)} \tag{21}$$

By deforming the integration path in (19) around these poles in the upper half of the complex t-plane (the integrand converges at infinity so as to make this

possible [2]) and invoking the residue theorem, one generates the residue series

$$\psi(x,y) = \frac{\pi}{\mu} \sum_{m=1}^{\infty} \frac{f_m(y')f_m(y)\exp(ixt_m)}{R_o(t_m)\frac{\partial}{\partial t}[R_o(t)R_i(t)]_{t_m}} \tag{22}$$

where

$$f_m(y) = Ai(\tau_m+\mu y) + R_o(t_m)Bi(\tau_m+\mu y) \tag{22a}$$

Each term in (22) represents a mode field $f_m(y)$ in the vertical cross section, which propagates along x with propagation coefficient t_m. The profile in (14) creates a surface duct between $y=0$ and $y=y_i$ because it is downward refracting in that height interval. For $y>y_i$, upward refraction takes place, with consequent leakage. The mode set t_m is therefore grouped into surface ducted (trapped) modes with small leakage ($\mathrm{Re}\, t_m > p(y_i)$), transitional modes ($\mathrm{Re}\, t_m \approx p(y_i)$), and leaky modes ($\mathrm{Re}\, t_m < p(y_i)$) (see Fig. 3). The estimates relating $\mathrm{Re}\, t_m$ to $p(y_i)$ are qualitative. Losses due to leakage out of the duct or due to a dissipative surface impedance Z_s are expressed by $\mathrm{Im}\, t_m$, which is positive; this controls the decay rate along x via the propagator $\exp(ixt_m)$ in (22), with larger values of $\mathrm{Im}\, t_m$ implying stronger damping.

C. Ray Expansion

The normal mode expansion in Section B is not always the most convenient for characterizing high frequency wave phenomena. An alternative is provided by a ray field expansion wherein local plane waves are tracked individually along direct and multiple reflected trajectories from source to observer [3,4]. Although the ray expansion can be phrased rigorously in terms of *generalized ray* spectral integrals, the principal utility of a ray field formulation rests in the asymptotic reduction of the generalized ray integrals, which yields the approximate fields that satisfy the rules of ray optics in inhomogeneous media. To generate the generalized ray series from the general result in (19), it is first necessary to decompose the oscillatory Airy functions Ai and Bi, which are natural descriptors of the (oscillatory) normal modes, into traveling wave form. Next, the resonant denominator $(1-R_oR_i)^{-1}$ in the integrand of (19) is removed by power series expansion, and the resulting integrand is rearranged into a sequence of combinations of traveling wave terms that form the generalized rays. Finally, asymptotic reduction produces the conventional ray fields.

Implementing the above scenario, we introduce the traveling wave Airy functions

$$w_{1,2} = Ai \mp iBi \tag{23}$$

and thereby rewrite (19) in the form

$$\Psi(x,y_<,y_>) = \frac{-1}{4\mu} \int_C \frac{\bar{h}(y_<,t)\bar{h}(y_>,t)}{1-\bar{R}_o(t)\bar{R}_i(t)} e^{ixt} dt \tag{24}$$

where

$$\bar{h}(y_<,t) = w_1(\tau+\mu y_<) + \bar{R}_o(t) w_2(\tau+\mu y_<) \tag{24a}$$

$$\bar{h}(y_>,t) = w_2(\tau+\mu y_>) + \bar{R}_i(t) w_1(\tau+\mu y_>) \tag{24b}$$

$$\bar{R}_o(t) = -\frac{\mu w_1'(\tau)+q w_1(\tau)}{\mu w_2'(\tau)+q w_2(\tau)} \quad , \quad w_{1,2}'(\tau) \equiv \frac{d}{d\tau} w_{1,2}(\tau) \tag{24c}$$

$$\bar{R}_i(t) = -\frac{\mu w_1(t-y_i) w_2'(\tau+\mu y_i) + w_1'(t-y_i) w_2(\tau+\mu y_i)}{\mu w_1(t-y_i) w_1'(\tau+\mu y_i) + w_1'(t-y_i) w_1(\tau+\mu y_i)} \tag{24d}$$

and

$$t - y_i = \mu^2(\tau+\mu y_i) \tag{24e}$$

Inserting the expansion

$$(1-\hat{R})^{-1} = \sum_{n=0}^{\infty} \hat{R}^n \quad , \quad \hat{R} = \bar{R}_o(t)\bar{R}_i(t) \quad , \tag{25}$$

into (24), and interchanging the order of summation and integration, one may order the resulting series as follows,

$$\Psi = \sum_{j=i}^{4} \Psi^{(j)} \quad , \quad \Psi^{(j)} = \sum_{n=0}^{\infty} G_n^{(j)} \tag{26}$$

where $G_n^{(j)}$, J=1...4, represents four species of generalized ray integrals (Fig. 4)

$$G_n^{(1)} = \frac{-1}{4\mu} \int_C w_1(\tau+\mu y_<) w_2(\tau+\mu y_>) \hat{R}^n e^{ixt} dt \tag{27a}$$

$$G_n^{(2)} = \frac{-1}{4\mu} \int_C w_2(\tau+\mu y_<) w_2(\tau+\mu y_>) \bar{\bar{R}}_o \hat{R}^n e^{ixt} dt \tag{27b}$$

$$G_n^{(3)} = \frac{-1}{4\mu} \int_C w_1(\tau+\mu_<) w_1(\tau+\mu y_>) \bar{R}_i \hat{R}^n e^{ixt} dt \tag{27c}$$

$$G_n^{(4)} = \frac{-1}{4\mu} \int_C w_2(\tau+\mu y_<) w_1(\tau+\mu y_>) \bar{\bar{R}}_o \bar{R}_i \hat{R}^n e^{ixt} dt \tag{27d}$$

The physical content of the generalized ray fields may be understood by employing asymptotic approximations in the integrands, and then evaluating the integrals by the saddle point method. For large values of their arguments, the Airy functions $w_{1,2}$ in (23) can be approximated by [5]

$$w_{1,2}(-\nu) \sim \mp i\pi^{-1/2}\nu^{-1/4} \exp\left(\pm i\frac{2}{3}\nu^{3/2}\right) \pm i\pi/4, \quad , \quad \mathrm{Re}\nu>0 \tag{28a}$$

$$w_{1,2}(\nu) \sim \mp i\pi^{-1/2}\nu^{-1/4} \exp\left(\frac{2}{3}\nu^{3/2}\right) \quad , \quad \mathrm{Re}\tau>0 \tag{28b}$$

Propagating ray fields are established by progressing phase terms as in (28a). Because of the different arguments of the various $w_{1,2}$ functions in (27), one must identify distinct t-intervals where these arguments have positive or negative real parts. For the present purposes, to obtain propagating ray fields, it is required that a) $\mathrm{Re}(\tau+\mu y_<)>0$, b) $\mathrm{Re}\,\tau<0$; but one may have c) $\mathrm{Re}(t-y_i)\gtrless 0$. As seen from (24d), the argument $(t-y_i)$ appears in the reflection coefficient due to the permittivity slope discontinuity at $y=y_i$. To distinguish the two cases, we append the subscript $\ell=1$ for $\mathrm{Re}(t-y_i)>0$ and $\ell=2$ for $\mathrm{Re}(t-y_i)<0$. The ray integrals $G_{\ell,n}^{(i)}$ pertaining to the spectral intervals C_ℓ defined by the constraints a), b) and $c_{1,2}$) are then reduced to the following forms (see Fig. 5 for typical trajectories):

$\underline{\ell = 1,\ l = 1}$

Here, via (28b), $\bar{R}_l(t) \sim -i$, which implies that the upgoing waves in this spectral interval are evanescent at $y=y_l$. Virtual reflection takes place at a level $y<y_l$, and the value (-i) of the reflection coefficient identifies an encounter with a caustic. Then,

$$G^{(1)}_{\ell=1,n} \sim \frac{-1}{4\pi} \int_{C_l} (-1)^n \Gamma^n(t;p(0);q)\ \frac{\exp\{ix\Phi^{(1)}_{1,n}(t)\}}{\{p(y_<)-t\}^{1/4}\{p(y_>-t\}^{1/4}} \qquad (29)$$

where

$$\Gamma(t;p(0);q) = -\frac{q-i\sqrt{p(0)-t}}{q+i\sqrt{p(0)-t}} \qquad (29a)$$

$$\Phi^{(1)}_{1,n}(t) = t+\frac{2}{3\mu^3 x}\left\{2n(p(0)-t)^{3/2} + (p(y_<)-t)^{3/2}-(p(y_>)-t)^{3/2}\right\} \qquad (29b)$$

The forms for $j= 2,3,4$ are similar. The saddle point $t^{(1)}_{1,n}$ of the integrand in (29) is located from the stationary phase condition

$$\frac{d}{dt}\Phi^{(1)}_{1,n}(t) = 0 \quad \text{at} \quad t^{(1)}_{1,n} \qquad (30)$$

which yields the solution

$$x = \frac{1}{\mu^3}\left\{2n(p(0)-t)^{1/2}+(p(y_<)-t)^{1/2}-(p(y_>)-t)^{1/2}\right\}_{t=t^{(1)}_{1,n}} \qquad (31)$$

Then by the conventional saddle point technique [6],

$$G^{(1)}_{1,n} \sim -\frac{1}{4}\sqrt{\frac{2}{\pi x Q^{(1)}_{1,n}}}\,(-1)^n\Gamma^n(t^{(1)}_{1,n};p(o);q)\ \frac{\exp\{ix\Phi^{(1)}_{1,n}(t^{(1)}_{1,n})+(i\pi/4)\mathrm{sgn}Q^{(1)}_{1,n}\}}{\{p(y_<)-t^{(1)}_{1,n}\}^{1/4}\{p(y_>)-t^{(1)}_{1,n}\}^{1/4}} \qquad (32)$$

with

$$Q^{(1)}_{1,n} = \frac{d^2}{dt^2}\Phi^{(1)}_{1,n}(t)\Big|_{t^{(1)}_0} = \frac{1}{\mu^3 x}\left\{2n\frac{1}{2\sqrt{p(0)-t}}+\frac{1}{2\sqrt{p(y_<)-t}}-\frac{1}{2\sqrt{p(y_>)-t}}\right\}_{t=t^{(1)}_{1,n}} \qquad (32a)$$

The saddle point condition in (31) is the equation for a ray path reflected n-times at $y=0$, the term Γ^n in (32) incorporates the associated reflection coefficient at $y=0$, the exponential term in (32) describes the phase accumulation along that path, $(-1)^n$ accounts for n ray encounters with a

caustic, and the remaining amplitude terms account for ray tube spreading.

$\underline{\ell = 2,\ 1 = 1}$

Now, from (28a)

$$\bar{R}(t) \sim i\hat{\Gamma}(t;\mu;y_i)e^{-i\frac{4}{3\mu^3}(p(y_i)-t)^{3/2}} \tag{33}$$

where

$$\hat{\Gamma} \sim \frac{\mu+\{w_1'(\mu^2\xi_i)/w_1(\mu^2\xi_i)\}\{w_2(\xi_i)/w_2'(\xi_i)\}}{\mu+\{w_1'(\mu^2\xi_i)/w_1(\mu^2\xi_i)\}\{w_1(\xi_i)/w_1'(\xi_i)\}}\ ,\ \xi_i = \tau+\mu y_i \tag{33a}$$

Then

$$G_{2,n}^{(1)} \sim \frac{-1}{4\pi}\int_{C_2}\Gamma^n(t;p(0);q)\hat{\Gamma}^n(t;\mu;y_i)\frac{\exp\{ix\Phi_{2,n}^{(1)}(t)\}}{\{p(y_<)-t\}^{1/4}\{p(y_>)-t\}^{1/4}}\,dt \tag{34}$$

where

$$\Phi_{2,n}^{(1)}(t) = t+\frac{2}{3\mu^3 x}\left\{2n\left[(p(0)-t)^{3/2}-(p(y_i)-t)^{3/2}\right]+(p(y_<-t)^{3/2}-(p(y_>)-t)^{3/2}\right\}\ , \tag{34a}$$

The saddle point condition yields

$$x = \frac{1}{\mu^3}\left\{2n\left[(p(0)-t)^{1/2}-(p(y_i)-t)^{1/2}\right]+(p(y_<)-t)^{1/2}-(p(y_>)-t)^{1/2}\right\} \tag{35}$$

and the asymptotic result

$$G_{2,n}^{(1)} \sim -\frac{1}{4}\sqrt{\frac{2}{\pi x Q_{2,n}^{(1)}}}\Gamma^n(t_{2,n}^{(1)};p(0);q)\hat{\Gamma}^n(t_{2,n}^{(1)};\mu;y_i)\frac{\exp\{ix\Phi_{2,n}^{(1)}(t_{2,n}^{(1)})+(i\pi/4)\mathrm{sgn}Q_{2,n}^{(1)}\}}{\{p(y_<)-t_{2,n}^{(1)}\}^{1/4}\{p(y_>)-t_{2,n}^{(1)}\}^{1/4}}, \tag{36}$$

$$Q_{2,n}^{(1)} = \frac{1}{\mu^3 x}\left\{2n\left\{\frac{1}{2\sqrt{p(0)-t}}-\frac{1}{2\sqrt{p(y_i)-t}}\right]+\frac{1}{2\sqrt{p(y_<)-t}}-\frac{1}{2\sqrt{p(y_>)-t}}\right\}_{t=t_{2,n}^{(1)}} \tag{36a}$$

Similar results can be derived for the other species $j= 2,3,4$, $\ell=1,2$.

The forms of the solution for $\ell = 1,2$ and $j=1$ in (32) and (36) are generic also for the other (ℓ,j) combinations. Thus

$$G_{\ell,n}^{(j)} \sim -\frac{1}{4}\sqrt{\frac{2}{\pi x Q_{\ell,n}^{(j)}}}\,\Gamma^n(t_{\ell,n}^{(j)};p(0);q)\hat{\Gamma}^n(t_{\ell,n}^{(j)};\mu;y_i)\,\frac{\exp[ix\Phi_{\ell,n}^{(j)}(t_{\ell,n}^{(j)})+(i\pi/4)\operatorname{sgn}Q_{\ell,n}^{(j)}]}{\sqrt{\Omega(y_<,t_{\ell,n}^{(j)})\,\Omega(y_>,t_{\ell,n}^{(j)})}} \tag{37}$$

$$\Omega(y,t) \equiv [p(y)-t]^{1/2} \quad . \tag{37a}$$

Here, Γ is defined in (29a), and $\hat{\Gamma}$ in (33a), for $\ell=2$, whereas $\hat{\Gamma}=-i$ for $\ell=1$. Moreover,

$$\Phi_{\ell,n}^{(j)} = t_{\ell,n}^{(j)}+\frac{2}{3\mu^3 x}\Big\{(2n+\alpha_1)\left[\alpha_2\Omega^3(0,t)-\alpha_3\Omega^3(y_i,t)\right]+\alpha_2'\Omega^3(0,t)$$
$$-\alpha_3'\Omega^3(y_i,t)+\alpha_4\Omega^3(y_<,t)+\alpha_5\Omega^3(y_>,t)\Big\}_{t_{\ell,n}^{(j)}} \tag{37b}$$

$$Q_{\ell,n}^{(j)}=\frac{1}{2\mu^3 x}\Big\{(2n+\alpha_1)\left[\alpha_2\Omega^{-1}(0,t)-\alpha_3\Omega^{-1}(y_i,t)\right]+\alpha_2'\Omega^{-1}(0,t)-\alpha_3'\Omega^{-1}(y_i,t)$$
$$+\alpha_4\Omega^{-1}(y_<,t)+\alpha_5\Omega^{-1}(y_>,t)\Big\}_{t_{\ell,n}^{(j)}} \tag{37c}$$

and the ray equation (saddle point condition) is

$$x=\frac{1}{\mu^3}\Big\{(2n+\alpha_1)\left[\alpha_2\Omega(0,t)-\alpha_3\Omega(y_i,t)\right]+\alpha_2'\Omega(0,t)-\alpha_3'\Omega(y_i,t) \tag{37d}$$
$$+\alpha_4\Omega(y_<,t)+\alpha_5\Omega(y_>,t)\Big\}_{t_{\ell,n}^{(j)}} \tag{37d}$$

Then the following definitions of the constants α_i, $i=1$ to 5, apply:

$\ell=1$, J=2: $\alpha_1=\alpha_2=-\alpha_4=-\alpha_5=1$, $\alpha_2'=\alpha_3'=\alpha_3=0$ (38a)

$\ell=2$, J=2: $\alpha_1=\alpha_3'=0$, $\alpha_2'=2$, $\alpha_3=-\alpha_4=-\alpha_5=1$ (38b)

$\ell=1$, J=3: $\alpha_1=\alpha_3=\alpha_2'=\alpha_3'=0$, $\alpha_2=\alpha_4=\alpha_5=1$ (38c)

$\ell=2$, J=3: $\alpha_1=\alpha_2'=0$, $\alpha_2=\alpha_4=\alpha_5=1$, $\alpha_3'=2$ (38d)

$\ell=1$, J=4: $\alpha_1=2$, $\alpha_2=-\alpha_4=\alpha_5=1$, $\alpha_3=\alpha_2'=\alpha_3'=0$ (38e)

$\ell=2$, J=4: $\alpha_1=2$, $\alpha_2=\alpha_3=-\alpha_4=\alpha_5=1$, $\alpha_2'=\alpha_3'=0$ (38f)

Typical ray paths are identified in Fig. 5. All of the asymptotic ray field results above are based on the valaidity of the asymptotic approximations in (28) for the integrand, and also on the validity of the isolated saddle point evaluation.

This excludes observation points near cautics, and also near glancing rays that are tangent to the refractive index slope discontinuity (duct boundary) at $y=y_1$ (Fig. 5).

D. Hybrid Ray-Mode Expansion

The most general format involving ray fields and mode fields is obtained by combining these self-consistently in a hybrid ray-mode expansion [4]. To generate the hybrid representation, we first deform the integration path C in (19) into the two contours C_ℓ, $\ell=1,2$, which surround, respectively, the trapped modes with $\mathrm{Re}\, t_m > p(y_i)$ and the leaky modes with $\mathrm{Re}\, t_m < p(y_i)$; these contours (Fig. 6) establish the rigorous complex extension of the real spectrum intervals associated with $\ell=1$ and $\ell=2$ in Section IV.C. Next, we expand the resonant denominator not into an infinite (ray) series as in (25) but into a truncated series:

$$\frac{1}{1-\hat{R}} = \frac{1}{1-\hat{R}} - \frac{1}{2}\frac{1+\hat{R}}{1-\hat{R}}\hat{R}^{N_2} - \frac{1}{2}\hat{R}^{N_2} + \sum_{n=N_2}^{N_1-1}\hat{R}^n + \frac{1}{2}\frac{1+\hat{R}}{1-\hat{R}}\hat{R}^{N_1} \qquad (39)$$

Then decomposing the attentuation function corresponding to C_1 and C_2 as in (26), one obtains

$$\psi = \sum_{j=1}^{4}\sum_{\ell=1}^{2}\psi_\ell^{(j)} \qquad (40a)$$

where

$$\psi_\ell^{(j)} = \sum_{n=N_2}^{N_1-1} G_{\ell,n}^{(j)} + \frac{1}{2}G_{\ell,N_1}^{(j)} - \frac{1}{2}G_{\ell,N_2}^{(j)} + R_{\ell,N_1}^{(j)} + R_{\ell,N_2}^{(j)} \qquad (40b)$$

Here, $G_{\ell,n}^{(j)}$ are the generalized ray integrals associated with C_ℓ, $\ell=1,2$, which have the integrands shown in (27). The remainder integrals $R_{\ell,N_i}^{(j)}$ have for each wave species $j=1$ to 4 the same integrand as the corresponding ray integral G_{ℓ,N_i}, but contain in the integrand the following additional factors:

$$R_{\ell,N_1}^{(j)}\colon\ M,\ M \equiv \frac{1}{2}(1+\hat{R})(1-\hat{R})^{-1}\ ,\ j=1 \text{ to } 4 \qquad (41a)$$

$$R_{\ell,N_2}^{(j)}\colon\ [\hat{R}^{N_2}(1-\hat{R})]^{-1} - M\ ,\ j=1 \text{ to } 4 \qquad (41b)$$

Asymptotic reduction of the ray integrals proceeds as in Section IV.C. The remainder integrals can be reduced by deforming the integration paths $C_{1,2}$ into steepest descent paths $SDP^{(j)}$ through the saddle point $t_{N_i}^{(j)}$ of the corresponding ray integral. Because each integrand contains the resonant denominator

$(1-\hat{R})^{-1}$, some of the modal pole singularities t_m are encountered during the deformation (Fig. 7) and contribute residue contributions that furnish partial modes ("partial" implies that the decomposed traveling wave spectra represented by w_1 and w_2 in the integrands contribute individually, instead of the full spectra expressed by the Ai, Bi functions in (22)). For $\ell=j=1$ and N_1 one obtains from deformation of C_1,

$$R^{(1)}_{1,N_1} = \sum_{m=1}^{M^{(1)}_{1,N_1}} G^{(1)}_m + R_{M^{(1)}_{1,N_1}} \tag{42}$$

where

$$G^{(1)}_m = \frac{\pi i}{2\mu} \frac{w_1(\tau_m+\mu y_<)w_2(\tau_m+\mu y_>)}{\frac{\partial}{\partial t}\bar{R}_o(t)\bar{R}_i(t)\,|_{t=t_m}} e^{ixt_m} \tag{42a}$$

is the partial mode field, and $R^{(1)}_{M^{(1)}_{1,N_1}}$ is a new remainder integral having the same integrand as $R^{(1)}_{1,N_1}$ but extending along $SDP^{(1)}_{1,N_1}$. For saddle point t_{N_1} separated from the modal pole $t_{M^{(1)}_{1,N_1}}$, the new remainder integral can be evaluated by the saddle point method to yield

$$R_{M^{(1)}_{1,N_1}} \sim \frac{i}{2} G^{(1)}_{1,N_1} \cdot \Gamma \tag{43}$$

where

$$\Gamma = \frac{1+\bar{R}_o(t)\bar{R}_i(t)}{1-\bar{R}_o(t)\bar{R}_i(t)}\bigg|_{t=t^{(1)}_{1,N_1}} \sim \frac{e^{-i\{\frac{2}{3}(-\tau)^{3/2}+\pi/4\}} - e^{i\{\frac{2}{3}(-\tau)^{3/2}+\pi/4\}}\Gamma}{e^{-i\{\frac{2}{3}(-\tau)^{3/2}+\pi/4\}} + e^{i\{\frac{2}{3}(-\tau)^{3/2}+\pi/4\}}\Gamma}\bigg|_{t^{(1)}_{1,N_1}} \tag{43a}$$

and

$$\Gamma = \Gamma(t;p(0);q) = -\frac{q-i\sqrt{p(0)-t}}{q+i\sqrt{p(0)-t}} \tag{43b}$$

For a perfectly conducting earth ($q=\infty$), (43) reduces to

$$R_{M^{(1)}_{1,N_1}} \sim \frac{i}{2} G^{(1)}_{1,N_1} \cot\left\{\frac{2}{3\mu^3}(p(0)-t^{(1)}_{1,N_1})^{3/2}+\pi/4\right\} \tag{44}$$

The contribution in (43) or (44) is usually small. When the saddle point is near the modal pole, the new remainder integral cannot be neglected and must be evaluated by uniform asymptotics in terms of incomplete error functions [].

For $\ell=j=1$, and N_2, the remainder integral is split into two parts (see (41b)). For the first term in (41b), the integration path C_1 is deformed around the enclosed pole singularities to generate a sum of modes as in (42a). For the second term in (41b), C_1 is deformed into $SDP^{(1)}_{1,N_2}$. This yields

$$R^{(1)}_{1,N_2} = \sum_{m=q}^{M} G^{(1)}_m - R_q \quad , \quad q \equiv M^{(1)}_{1,N_2} \tag{45}$$

The integral R_q is the same as the one for $R^{(1)}_{1,N_2}$ arising from the second term of (41b), except that the integration path is $SDP^{(1)}_{1,N_2}$. Therefore, the evaluation of the integral can proceed as above. The same scenario can be repeated for all of the other integrals $R^{(j)}_{\ell,N_1}$. Details are given in Appendix A. When all of these results are combined, one obtains the following most general hybrid ray-mode representation of the attenuation function:

$$\psi = \sum_{j=1}^{4} \sum_{\ell=1}^{2} \left\{ \sum_{n=N_2}^{N_1-1} G^{(j)}_{\ell,n} + \frac{1}{2} G^{(j)}_{\ell,N_1} - \frac{1}{2} G^{(j)}_{\ell,N_2} \right\}$$

$$+ \sum_{j=1}^{4} \sum_{m=1}^{M^{(1)}_{1,N_1}} G^{(j)}_m + \sum_{j=1}^{4} \sum_{m=M^{(\ell)}_{1,N_2}}^{M^{(\ell)}_{2,N_2}} G^{(j)}_m + \sum_{j=1}^{4} \sum_{m=M^{(\ell)}_{2,N_1}}^{\infty} G^{(j)}_m$$

$$+ \sum_{j=1}^{4} \sum_{\ell=1}^{2} \left\{ R_{M^{(\ell)}_{\ell,N_1}} - R_{M^{(\ell)}_{\ell,N_2}} \right\} \tag{46}$$

This expansion is *exact* if the generalized ray integrals and all remainder integrals are kept intact, but useful results are obtained by employing the asymptotic reductions discussed earlier.

References

[1] J.R. Wait, *Electromagnetic Waves in Stratified Media,* Pergamon Press, New York, pp. 107-137, pp. 341-363 (1962).

[2] V.A. Fock, *Electromagnetic Diffraction and Propagation Problems,* Pergamon Press, New York, pp. 254-275 (1965).

[3] A.V. Kukushkin and V.G. Sinitsin, "Rays and Modes in a Nonuniform Troposphere," Radio Science, Vol. 18, No. 4, pp. 573-587 (1983).

[4] T. Ishihara and L.B. Felsen, "Hybrid (Ray)-(Parabolic Equation) Analysis of Propagation in Ocean Acoustic Guiding Environments," J. Acoust. Soc.

Am., to be published.

[5] A. Abramowitz and I.A. Stegun, *Handbook of Mathematical Functions,* Dover Publications, pp. 437-478 (1972).

[6] L.B. Felsen and N. Marcuvitz, *Radiation and Scattering of Waves,* Prentice-Hall, Inc., New Jersey, pp. 399-406 (1972).

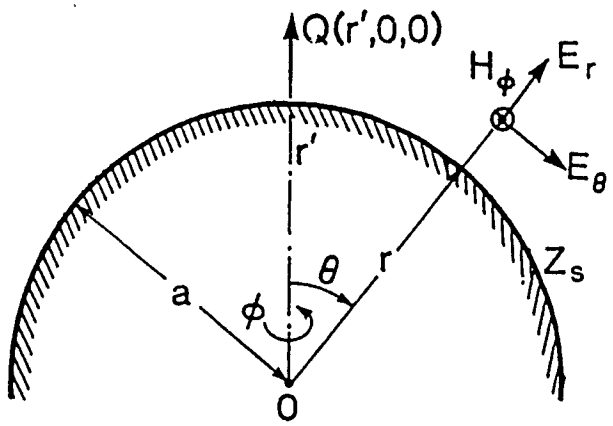

Fig. 1 Spherical earth (radius r= a) with vertical electric dipole source at Q. (r,θ,ϕ) are spherical coordinates, and the excited field components are E_r, E_θ, H_ϕ.

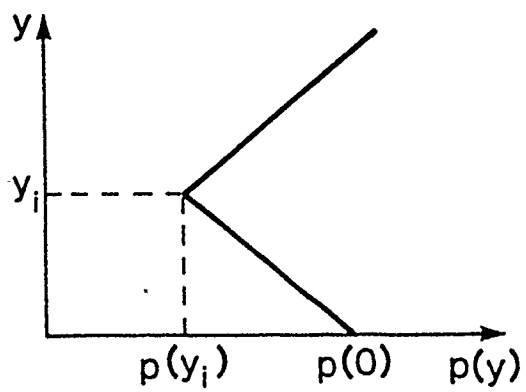

Fig. 2 Bilinear permittivity profile corresponding to (10) and (14).

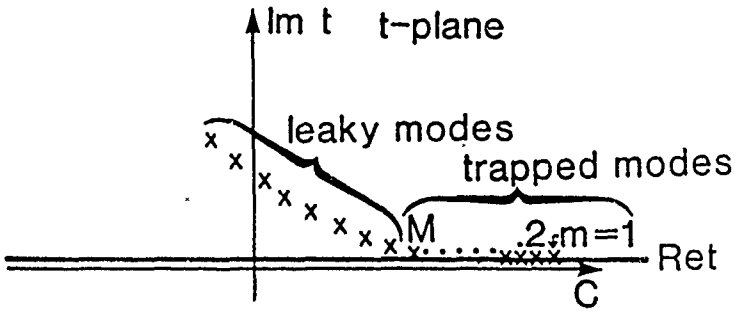

Fig. 3 Qualitative placement or singularities (for low loss surface conditions) and integration path for (19) in complex t-plane. Trapped and leaky mode ranges correspond roughly to $\mathrm{Re}\, t_m > p(y_i)$ and $\mathrm{Re}\, t_m < p(y_i)$, respectively, where y_i locates the upper boundary of the duct. m= mode index.

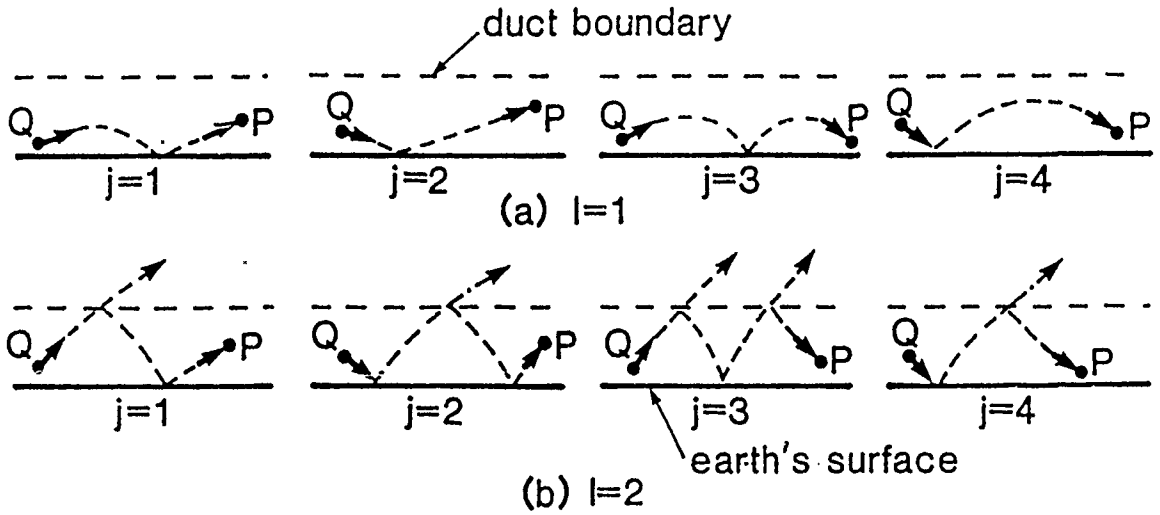

Fig. 4 Ray species $j=1 \cdots 4$ for categories $\ell=1$ (trapped inside duct) and $\ell=2$ (leaking out of duct). For arbitrary reflection index n, the ray species are organized according to their directions of departure from Q and arrival at P.

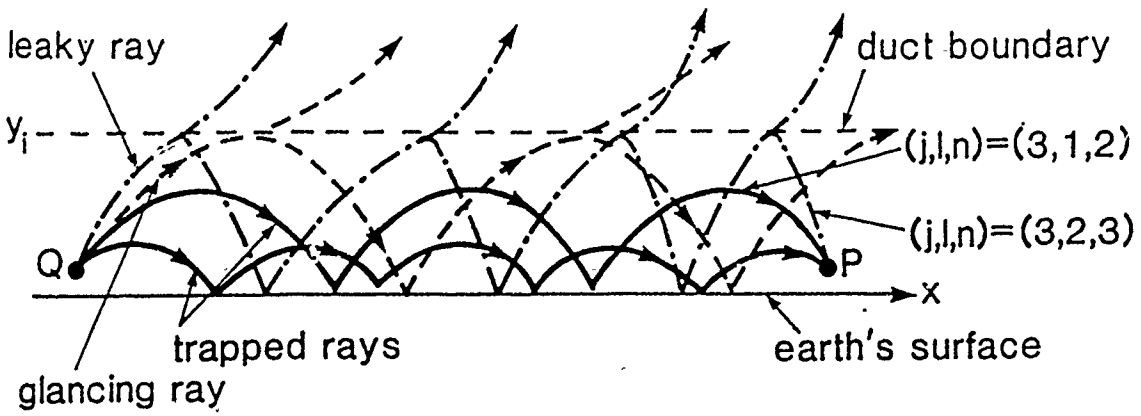

Fig. 5 Typical ray trajectories categorized as in Fig. 4. Trapped rays ____; leaky rays – ·– ·– ; glancing rays ---.

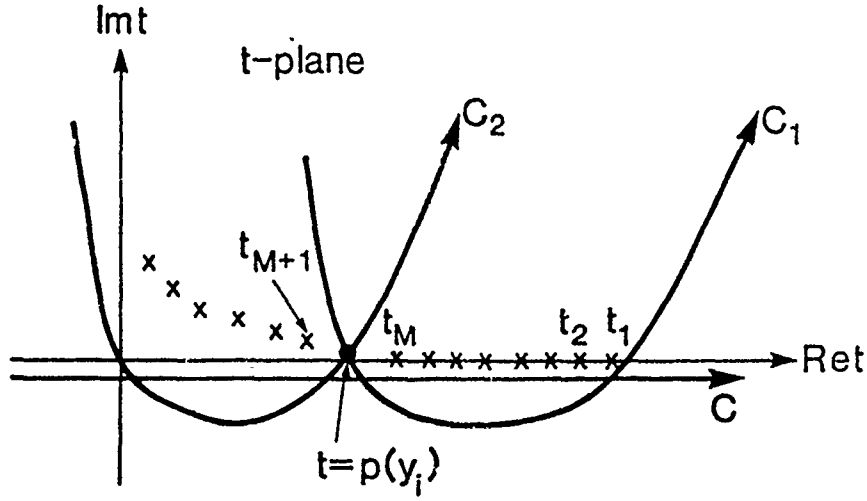

Fig. 6 Deformed integration contours preliminary to hybrid ray-mode expansion. C_1 and C_2 enclose the trapped and leaky modes, respectively.

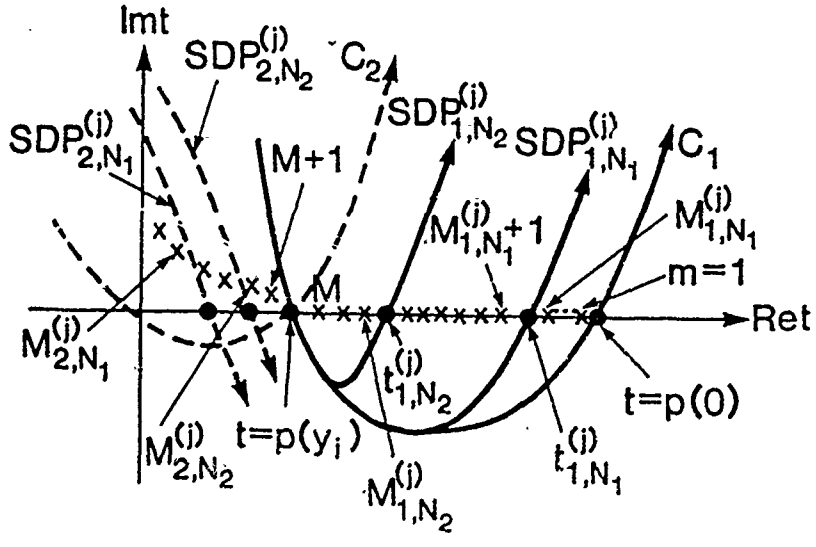

Fig. 7 Hybrid ray-mode expansion by deformation of integration contours C_1 and C_2 into steepest descent paths $SDP^{(j)}_{\ell,N}$ through the saddle points $t^{(j)}_N$ of the remainder field integrands. Mode contributions arise from poles crossed during the deformation.

APPENDIX A

DOCTRINE.C MAINTENANCE DESIGN NOTES

The AEGIS doctrine parser is designed to provide a high degree of operational flexibility without burdening the human operator. This flexibility could easily permit a DOCTRINE derivative to be used to extract information of any potential use as long as the information is preceded by a well-defined trigger phrase.

The syntax to use DOCTRINE follows:

DOCTRINE [doctrine-file-name [message-source [trigger-phrase]]]

DOCTRINE is intended to be run in background mode; it requires no additional action on the part of the user. During operation, the program scans messages arriving over a serial port until AEGIS doctrinal information is received. The doctrinal information is then stored into a file. This process continues indefinitely.

To make operation as easy as possible on the user, default values for the command line parameters are assumed if none are provided. The following defaults are hard-wired in function READ_ARGUMENTS of DOCTRINE.C:

"destination" -- Where is the extracted doctrine information to be stored? If no "doctrine-file-name" is provided on the command line, DOCTRINE sends its extractions to "" (empty string).

"msgsource" -- Where is the information to be received? If no "message-source" is provided on the

command line, DOCTRINE attempts to read the "/dev/ttyb" serial port.

"trigger" -- What phrase is used to indicate the start of AEGIS doctrine in the message? If no "trigger-phrase" is provided on the command line, DOCTRINE uses "XXXAEGISDOCXXX".

In order to provide the greatest flexibility, DOCTRINE searches for occurrences of "trigger-phrase" in the incoming message stream. This not only avoids the slower finite-state approach, but also permits any number of ways that the doctrine message could be formatted ("NOTE", "NARRATIVE", "REPLY", "TEXT", etc.). This disadvantage to this approach is that ANY occurrence of the trigger-phrase initiates extraction. Consequently, messages that discuss the trigger phrase but do not actually contain doctrinal information should not be passed to the parser.

The particular algorithm that DOCTRINE uses to detect the trigger is fast, but not particularly robust. It can miss some occurrences of the trigger when the trigger is preceded by a partial phrase that looks like the trigger. Fortunately, this is not possible with the default trigger. However, if the trigger were "ABABAC", then any doctrine information following the line that contains "ABABABAC" would be missed -- even though the trigger phrase is present. The scanning algorithm does have some robustness so that inadvertently duplicated characters would be ignored. ("XXXAAEEGGIISSDDOOCCXXX" would trigger extraction in the default case.)

In its delivered form, DOCTRINE discards all characters that follow the trigger phrase on the same line. That is, the

doctrinal information is presumed to start on the line FOLLOWING the trigger phrase. If the information that immediately follows the trigger needs to be extracted, that can be accomplished by commenting out the logic branch in function READ_TTY that begins "if (trigstat==0)". (The integer "trigstat" provides an indication of how much of the trigger phrase has been read. It is negative if not all the phrase has been found. It is incremented as each received character is matched against the trigger phrase in memory. When "trigstat" becomes 0, a match of the trigger phrase has been found.)

After the end-of-line that follows the trigger phrase has been received, DOCTRINE stores all new characters received into the doctrine-output-file until a slash ("/") character is received. The assumption used is that no slash character will be embedded within the raw doctrine information. (If this turns out not to be the case, the process for determining the end-of-doctrine will be more complicated. For instance, a particular character, even a slash, can be used to prefix all doctrine lines in the formatted message. A more-straight-forward, but less flexible, approach is to merely copy a specific number of characters.) With the slash character as end-of-doctrine, the output doctrine file could contain a formatting keyword (such as "ENDAT"). The end-of-doctrine character is hardwired into the "read_tty" function at the line "else if (ch=='/') {".

By adjusting the output file, the input source, the trigger phrase, the start-of-data (end-of-line by default) and the end-

of-data ("/" by default) definitions, DOCTRINE can be modified to extract any type or amount of data from formatted messages.